THE ASTROPHYSICAL JOURNAL, 269:182–201, 1983 June 1

EINSTEIN OBSERVATIONS OF THE RHO OPHIUCHI DARK CLOUD: AN X-RAY CHRISTMAS TREE

THIERRY MONTMERLE AND LYDIE KOCH-MIRAMOND
Section d'Astrophysique, Centre d'Etudes Nucléaires de Saclay, France
EDITH FALGARONE
Département de Radioastronomie Millimétrique, Observatoire de Meudon, France[1]
AND
JONATHAN E. GRINDLAY[2,3]
Harvard-Smithsonian Center for Astrophysics
Received 1982 August 19; accepted 1982 November 10

ABSTRACT

An extensive Guest Observation of the ρ Ophiuchi dark cloud region was conducted with the *Einstein Observatory*, featuring in particular repeated observations of several parts of the cloud, on time scales down to a day, or even hours. In all, 14 IPC and 3 HRI fields were obtained. Initially motivated by a search for a possible compact counterpart to the *COS B* γ-ray source 3CG 353+16 (for which no evidence was found), the present study gave a wealth of data, which turned out to be mostly relevant to early stages of stellar evolution.

Among the most significant results are the following:

1. About 50 weak sources were discovered in the $2° \times 2°$ area investigated. There is some evidence for up to 20 more sources.
2. These sources form a class of X-ray sources, which are most likely pre–main-sequence or very young objects; only ~one-half of them are known to be so at present from "standard" criteria (optical, IR, etc.).
3. Most sources are highly variable, largely beyond what could be caused by unknown gain fluctuations. Variability factors may reach one order of magnitude or more in a day.
4. The overall distribution of the normalized amplitude variations follows a power law.

We interpret the time variability in terms of strong stellar flares, which dominate the X-ray luminosity of the sources (this is the case in particular for the 9 T Tauri stars we detect, out of the 11 contained in the investigated area.) In one extreme case, we may even have observed the strongest stellar X-ray flare ever recorded.

Finally, we discuss several implications bearing on early stages of stellar evolution and some consequences of the presence of X-ray active objects within dark clouds. Several comparisons are made with the Orion complex. Possible observational tests are suggested.

Subject headings: gamma rays: general — nebulae: individual — stars: flare — stars: pre–main-sequence — X-rays: sources

I. INTRODUCTION

a) *Motivation*

The ρ Oph dark cloud region has been extensively investigated at various wavelengths. Optical, radio, and IR observations point to the presence of very young objects, like T Tauri stars, and early-type stars having very recently reached the main sequence (e.g., Falgarone 1979; Elias 1978, and references therein). In the high-energy range, the first results were those of the *COS B* satellite (Scarsi *et al.* 1977), which discovered a weak γ-ray source in the direction of the cloud, 2CG 353+16 (Swanenburg *et al.* 1981). On the basis of existing estimates of the mass of the cloud, especially from CO measurements, it was found that the γ-ray flux resulting from the interaction of average density cosmic-ray protons and electrons with the cloud (via $\pi°$ decay and bremsstrahlung, respectively) fell short of the observed flux by a factor ~5. Particle acceleration within the cloud, or in its immediate vicinity, was then suggested by several authors to account for the excess γ-ray flux (e.g., Bignami and Hermsen 1982 and references therein), contrary to what is thought to take place, for instance, in the Orion Nebula, where no such excess is observed (Caraveo *et al.* 1980).

However, one cannot *a priori* rule out that a compact object (like an unknown pulsar or a black hole) on the line of sight—or inside—the cloud, may instead be the

[1] Also at Laboratoire de Physique de l'Ecole Normale Supérieure, Paris.
[2] Alfred P. Sloan Foundation Fellow.
[3] Visiting Astronomer, Cerro Tololo Inter-American Observatory, which is operated by the Association of Universities for Research in Astronomy, Inc., under contract with the National Science Foundation.

actual counterpart to the γ-ray source. An observation program using the Imaging Proportional Counter (IPC) aboard the *Einstein Observatory* (Giacconi *et al.* 1979, 1981) was set up to map the *COS B* error box and to look for the possible X-ray signature of such a counterpart.

The *COS B* error box, a circle of $\sim 1°$ radius, was covered by a mosaic of 5 IPC fields, the "middle" field (i.e., centered on the middle of the *COS B* error circle) overlapping the four other, mutually adjacent fields. This mosaic was the subject of two set of observations, made 6 months apart in 1979, which showed not merely one but at least a dozen weak sources in the immediate vicinity of the molecular cloud, some of them being highly variable (Montmerle, Koch-Miramond, and Grindlay 1981*a*, *b*). On the basis of preliminary identifications with pre–main-sequence (PMS) objects (including one T Tauri star), several follow-up IPC and HRI (High Resolution Imager) observations were made, separated by only 1 or 2 days. Altogether, the 14 IPC and 3 HRI exposures thus obtained make up a unique investigation, in both space and time, of the ρ Oph dark cloud region. The analysis of the data, covering a $\sim 2° \times 2°$ area, led to the discovery of about 50 distinct sources, almost all variable, and up to 20 weaker sources.

b) *Outline of the Paper*

In this paper, we mainly discuss the results obtained on the field centered on the densest part of the cloud (hereafter the "center" field), which was the target of six repeated IPC observations made at various epochs, and three spatially distinct HRI observations.

After having briefly described the observations and some specific features of the data analysis (§ II), we discuss the space distribution of the sources (§ III), emphasizing their specific nature as highly variable X-ray objects (§ IV). Because variability turned out to be particularly remarkable in one source, we discuss in more detail the corresponding observations (§ V) and focus on a very strong event, for which arguments in favor of a flare interpretation are given (§ VI).

A discussion of the results in a more general framework is presented in § VII, and main conclusions are drawn in § VIII.

II. OBSERVATIONS AND ANALYSIS

a) *Source Detection*

The standard data processing led to the detection of about 20 sources in the *COS B* error circle, with effective exposures ~ 1600–2500 s for the IPC, and $\sim 11{,}000$–$12{,}000$ s for the HRI. However, the sources were not always present in separate images, and strong variability was clearly a general trend from the outset. As an illustration, we present in Figure 1 the contour maps corresponding to the six IPC exposures of the center field, normalized to 2000 s.

Owing to the complex structure of the IPC images (blended sources and sources away from the axis), the detection of weak sources by the standard processing is difficult. For instance, there is no source in the middle of the "center" field, where the detector is best known, and a majority of sources lie in the annulus from which the standard background is estimated, thus raising it artificially. Therefore, on the basis of the contour maps, a number of candidate sources were studied using interactive processing programs. Their background, taken from a nearby area free from sources, as well as their detection radius, were generally different from one source to the next, but were also varied in several cases to check the consistency of the results. This treatment allowed us to push down the detection limit when a weak source (for instance, detected below 2σ in a single observation and thus usually discarded) was seen repeatedly. In the center field, the best lower limit (2σ) achieved was 3×10^{-3} counts s^{-1} in the total IPC passband, i.e., a luminosity of 3×10^{29} ergs s^{-1} (see § III*d*); in general, this lower limit corresponds to 5 counts during one exposure.

b) *Variability*

Count rate variations can be caused simply by unknown gain changes from observation to observation, or from pixel to pixel if the observation axes and roll angles are not exactly identical. This is because the gain is not known accurately beyond the first 4′ off the axis (Gorenstein, Harnden, and Fabricant 1981). In principle, this is a problem for us, since most sources lie at least $\sim 10'$ or $20'$ away. However, in almost every case, the spectral distribution of the counts is very deficient in low-energy photons (< 1 keV) (see § III*d*), so that a shift in the relationship between pulse height channel and energy, corresponding to a gain variation, does not affect the total number of counts in the IPC passband (i.e., the source flux). Specifically, in most cases, the difference in total counts resulting from a possible shift of ± 2 units in the Al peak channel monitoring the gain remains within the statistical uncertainties, after removal of the background. An extreme shift of ± 3 units broadens the uncertainties but does not affect the results significantly. In addition, many observed count rate variations are large (at least a factor of 2, and up to an order of magnitude; see § IV*b*), and include increases as well as decreases. Also, vignetting corrections cannot introduce an erroneous variability, since the roll angles of the various sets of images differ usually by much less than 1°.

In view of all these arguments, we conclude that the variations we observe must be real when they are larger than the statistical uncertainties.

III. SPACE DISTRIBUTION AND NATURE OF THE SOURCES

a) *Overview*

The overall distribution of the sources in the "center" region is shown on a merged image of the six IPC observations, superposed on a Palomar Sky Survey red print (Fig. 2 [Plate 1]). There are apparently diffuse structures (in particular near the remarkable concentration of stars around $\alpha \approx 16^h23^m20^s$, $\delta \approx -24°15'$), which

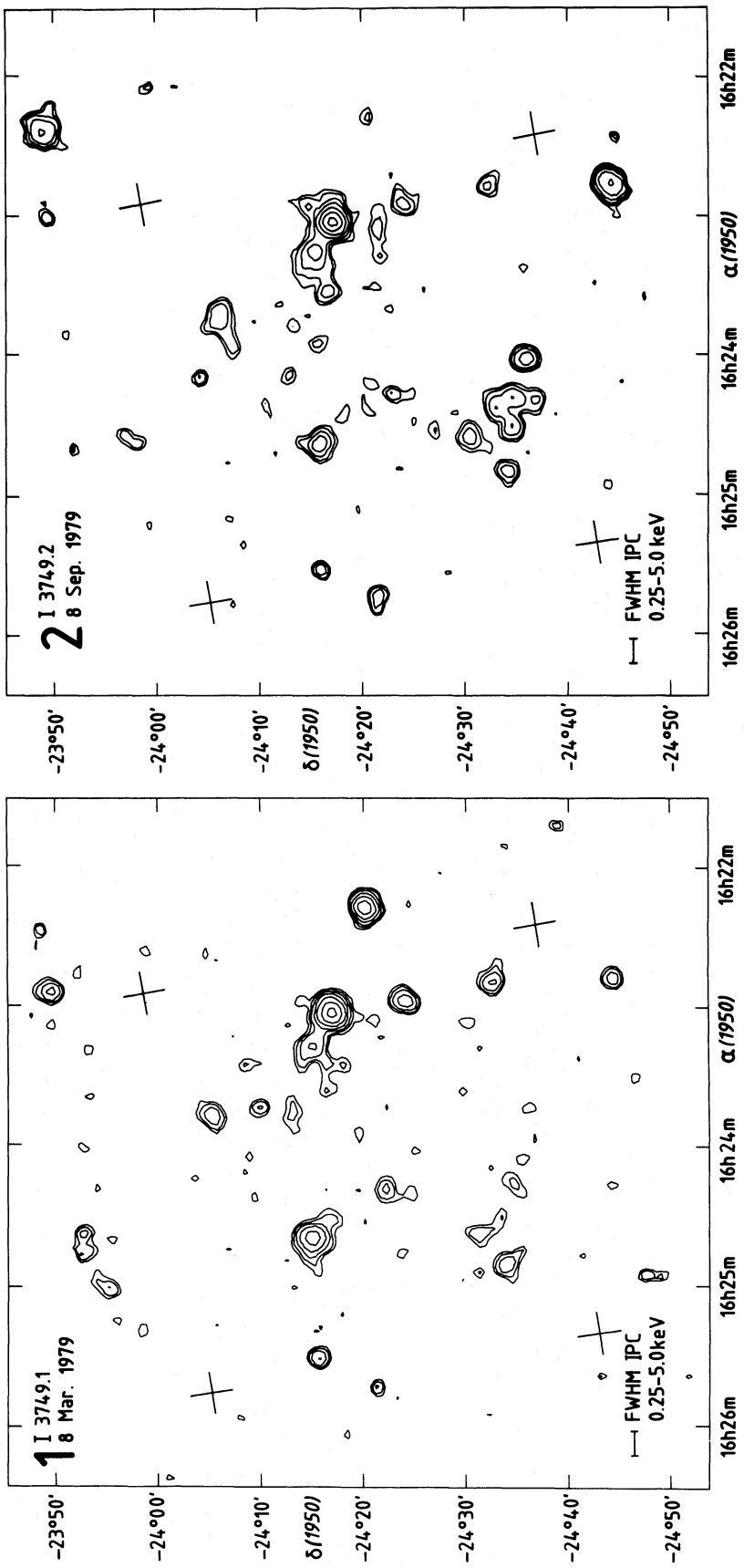

FIG. 1*a*

FIG. 1.—Contour maps of the six IPC exposures of the "center" field of the ρ Oph dark cloud. The IPC reference number, as well as the observation dates, are indicated. The maps are the result of a convolution of the count distribution with a Gaussian profile, 30″ HWHM. The contours are normalized to a 2000 s exposure; contour $(n-1)$ is $2 \times (1.5)^n$ σ above standard background. The crosses refer to the intersection of the IPC ribs. (Maps 1 and 2 are slightly different from those published in Montmerle, Koch-Miramond, and Grindlay 1981*a* because of the use of a revised processing.) Note the time intervals: 6 months (Fig. 1*a*); 17 months, 1 day (Fig. 1*b*); 2 days, 2 days (Fig. 1*c*).

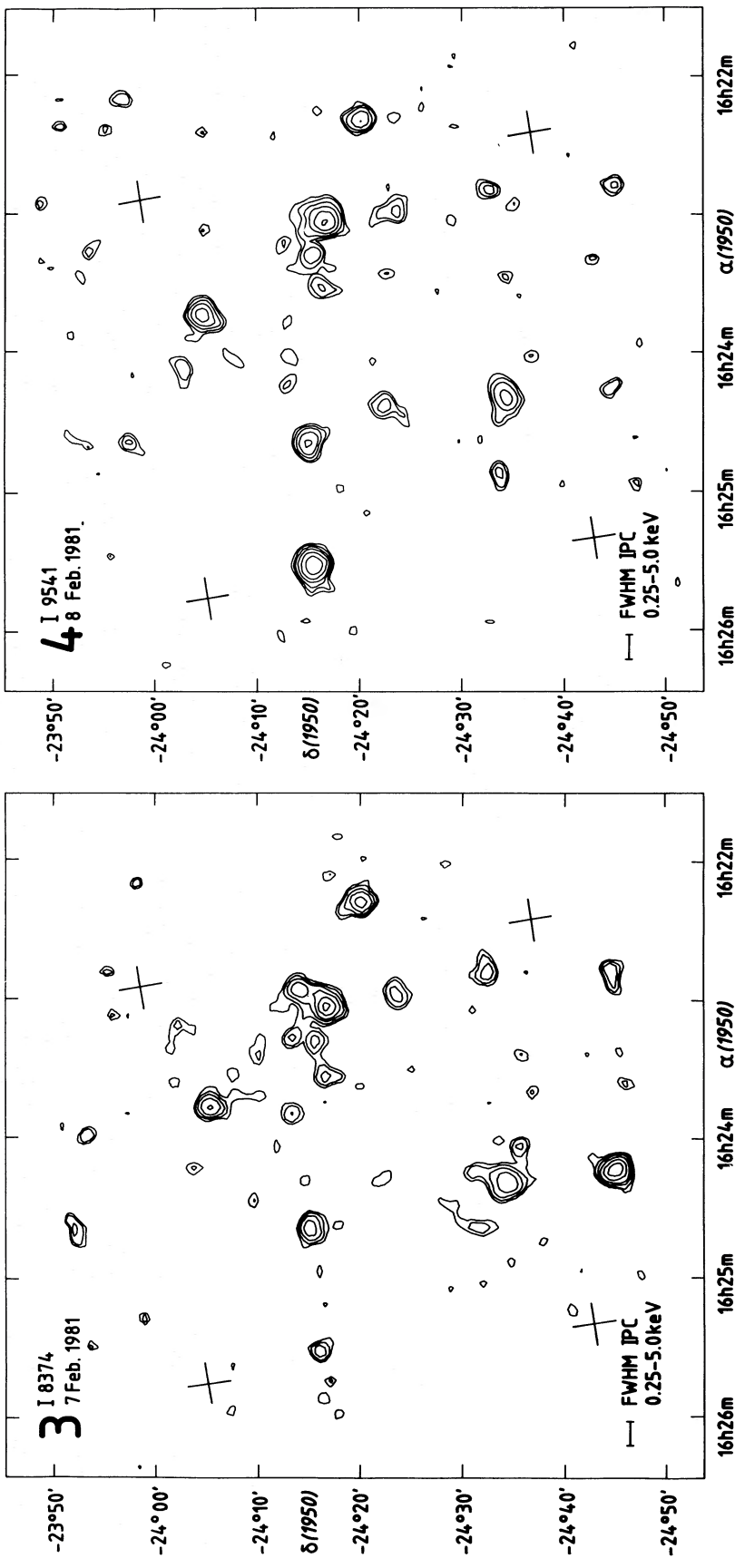

FIG. 1*b*

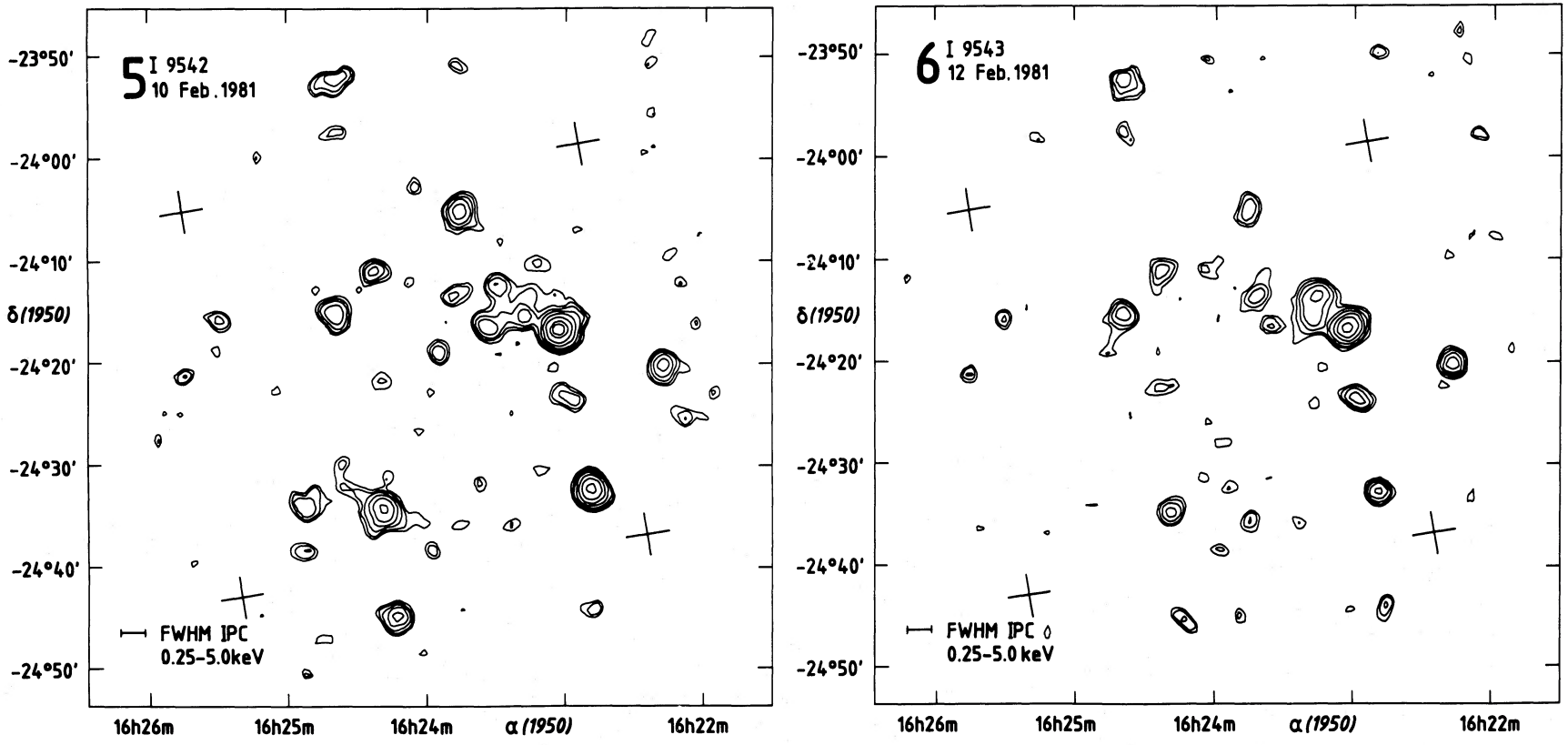

FIG. 1c

were noticed by Montmerle, Koch-Miramond, and Grindlay (1981*a*) in the first two observations. These structures can in fact be resolved into several variable sources (see Fig. 1). In this area the HRI image shows only one source, which is locally the brightest IPC source, by at least a factor of 3. The roughly annular structure of the source distribution in Figure 2 is intriguing. In fact, it closely follows the densest parts of the cloud in this region, where the visual absorption exceeds ~ 8 mag over an area $\sim 10'$ in radius, centered at $\alpha \approx 16^h23^m20^s, \delta = -24°25'$ (see Encrenaz, Falgarone, and Lucas 1975). In the same region, but in a more localized area (5′ radius), around $\alpha = 16^h23^m46^s$, $\delta = -24°25'44''$, Lada and Wilking (1980) have found evidence for ^{13}CO self-absorption, implying there is a visual absorption of more than 100 mag.

Since in order to be detected by *Einstein*, the sources must have absorption column densities typically below a few times 10^{22} cm^{-2}, only the sources about the periphery of the densest regions of the cloud are expected to be visible (see also below, § III*d*). Hence, the ring structure could be explained, at least in part, by absorption effects linked to the matter distribution.

The whole $2° \times 2°$ area covering the *COS B* error circle is shown in a similar way, on two figures (Figs. 3*a* and 3*b* [Plates 2 and 3]), corresponding to two observations separated by several months. Variability can also be seen for many sources. As a whole, the strong sources appear to be grouped in the upper half of the figure, when the absorption is greatest, confirming the trend noted in the center region.

A detailed discussion of the correlation between the distribution of the X-ray sources and of the dense matter will be presented elsewhere.

b) *Source Lists*

About 30 resolved sources are clearly visible in the "center" field (Fig. 2). In addition, 16 sources are detected in the adjacent fields, by the same method as described above. Altogether, we give in Table 1 a list of 47 sources detected above 3.5 σ in the $\sim 2° \times 2°$ area covering the *COS B* error box. These sources will be referred to as the "ROX" (Rho Oph X-ray) sources and are discussed extensively in this paper. In the "center" field, it is even possible to draw a complementary list of 20 candidate sources, detected above 2σ (Table 2). Normally, one would have discarded these sources, but a remarkably high fraction (more than 50%) have possible counterparts at other wavelengths, as do the ROX sources.

In addition, several sources are also seen by the HRI, and several are seen repeatedly by the IPC, albeit with a very low statistical weight in each observation. Nevertheless, it is likely that a few sources are only statistical fluctuations. As to variability, owing to the small number of counts detected in these sources, it is clearly impossible to give any significant estimate.

Other such candidate sources with a low statistical significance do appear also in the fields adjacent to the "center" field (Figs. 3*a* and 3*b*). However, the number of repeated observations (2) is too low to assess the reality of the corresponding features, which can only be established with future observations.

In what follows, the discussion will deal only with the ROX sources.

c) *Identifications*

Thirty out of the 47 ROX sources have possible counterparts in one or several surveys (optical, Hα, near-IR, radio continuum; see references in Table 1), while 17 have no such identification ($\sim 30\%$). Only five have no optical counterpart on the PSS red print.

Several findings may be pointed out.

1. Out of 11 T Tauri stars known in the $2° \times 2°$ field investigated, *nine* (80%) *are detected*, a much higher proportion than the $\sim 30\%$ previously found (e.g., Walter and Kuhi 1981). The two undetected T Tauri stars have the smallest optical luminosities (see Cohen and Kuhi 1979; see also discussion in § VII*c*).

2. Out of eight emission-line stars found by Struve and Rudkjøbing (1949), six (75%) are detected.

3. Out of 19 near-IR sources associated with the cloud, according to Elias (1978), 15 (80%) are detected.

4. As part of a preliminary investigation of the optical properties of ROX sources previously unknown optically, one of us (J. E. G.) obtained spectra in 1980 May on three new stars, using the 4 m telescope at Cerro Tololo Interamerican Observatory and the SIT vidicon detector. All show Hα emission; as an example, the spectrum of ROX 3, typical of a late-type PMS star, is shown on Figure 4. A similar finding has been reported for several stars by Feigelson and Kriss (1981), and by Walter and Kuhi (1981), in the Taurus-Auriga complex. The above characteristics, together with the spatial distribution of the ROX sources, which follows rather closely the dense matter distribution (§ III*a*), strongly suggest that, as a whole, *the ROX sources are PMS objects*, or at least, very young objects, such as early B stars surrounded by compact H II regions. Thus, as seen from the X-ray data, there could be up to 2 times more PMS objects in the cloud than previously known (see Table 1), in the regions where the absorption does not forbid soft X-rays to leak out.

However, there is no evidence for a compact counterpart to the γ-ray source 2CG 353+16, emitting X-rays by strong accretion from a companion, or from the presumably dense circumstellar cloud material. Although unlikely, the possibility remains that an absorbed source of this kind lies in the densest parts of the cloud. A possible test is as follows. It has been recently suggested by McCray (1982) that strong molecular hydrogen line emission might be expected from the periphery of an X-ray heated ionization zone (such as considered by Halpern and Grindlay 1980), around an accretion source embedded in a cloud. Deep high resolution maps of the ρ Oph cloud in the ~ 2 μm vibrational lines of H_2 would be very useful. But of course the X-ray counter-

TABLE 1

RHO OPHIUCHI X-RAY SOURCES ($< 3.5\ \sigma$)

ROX #	det	α(1950) h m s	δ(1950) ° ' "	IPC pos. class	min. counts ($10^{-3}s^{-1}$)	obs #	max. counts ($10^{-3}s^{-1}$)	obs #	Δt min	σ comb	optical id. list or PSS	optical id. m	near IR id. GSS	VS	VSS	C	E	Radio cont.	A_V	Spectral type	Ref	Hα EW (Å)	Ref	Remarks
(1)	(2)	(3)		(4)	(5)	(6)	(7)	(8)	(9)	(10)	(11)	(12)	(13)	(14)	(15)	(16)	(17)	(18)	(19)	(20)	(21)	(22)	(23)	(24)
1	I	16 22 18	-24 20 10	c	5 ± 2	2	63 ± 7	1	6m	14	SR2	9.3	5	-	-	1	6	-	1.0-2.4	A2V-B9V	C			Field star ?
	H	16 22 18.1	-24 20 01.6	-																G8	E			(double)
2	I	16 22 24	-23 48 42	c	< 11	6	64 ±12	2	17m	5.0	⊡	15.3	:	:	20	:	U	-	[4.7]/1.5	M	G	2.5	G	New PMS star
3	I	16 22 47	-24 44 11	c	8 ± 3	5	63 ± 8	2	2d	11	⊡	13.2	:	:	-	:	-	-	1.2	M	G	3.1	G	New PMS star
4	I	16 22 49	-24 32 19	a	9 ± 3	4	75 ± 7	5	2d	14	✳	(14.5)	:	:	23	:	-	-						
5	I	16 22 54	-23 49 23	c	< 12	6	32 ± 7	1	23m	4.6	⊡	(14.0)	:	:	-	:	-	-						
6	I	16 22 56	-24 14 19	a	< 5	6	24 ± 4	3	1d	6.4	SR4=DoAr20	12.7v	-	-	-	-	13	-	2.1	K7	CK	84	CK	T Tauri
7	I	16 22 57	-24 23 31	a	11± 3	5	20 ± 4	1	2d	9.3	⊡ + 1	(16.0)	20	-	-	-	U	-	13		VS			
	H	16 22 55.1	-24 23 52.1	-																				
8	I	16 23 03	-24 16 59	a	59± 7	3	132 ± 9	5	3d	29	DoAr21	14.1v	23	-	-	7	14	OPH10	10	B2V	C	<0.5	G	Hα detected
	H	16 23 01.8	-24 16 49.0	-															6	G5III-KOIII	C			by Do Ar, not
																				B3V	FG			detected later
																			9		VS			
9	I	16 23 12	-25 35 55	b	< 13	B	13 ± 3	A	(17m)	4.1	3(Δm=5)	(12.5)	:	:	:	:	-	:						
10	I	16 23 16	-24 12 59	a	< 5	5	34 ± 4	6	2d	8.6	DoAr24	14.6	28	-	-	10	19/20	-	6.2-7.8	B9V-A0V	C	Y	DoAr	T Tauri
											DoAr24E	(12.0)	31	-	-	13	21/22	-	9.2-10.8	B3V-B5V	C			(Footprint area)
											1	(16.5)							6.9	G8III				
11	I	16 23 18	-24 15 32	a	10± 4	3	40 ± 6	2	5d	12	-	-	29	-	-	11	18	-	15-17	B8-B5V	C			T Tauri
12	I	16 23 22	-25 20 44	b	33± 5	A	47 ± 9	B	(17m)	8.5	2⊡+2(Δm=3)	(13.5)	:	:	-	:	-	:						
13	I	16 23 28	-24 13 00	a	< 4	6	11 ± 3	5	2d	3.8	⊡(Δm=4.5)	(12.0)	-	-	-	-	-	-						
14	I	16 23 34	-24 16 36	a	5± 2	6	17 ± 3	5	2d	7.6	⊡	(16.5)	35	-	-	15	25	OPH4	7.4-8.0	F2V-A7	C			IR source 1
																				B3V	FG			of GSS
																			10.9	B2	CK	-		PMS object
15	I	16 23 41	-24 13 41	a	< 5	5	8 ± 2	6	2d	3.8	✳	(17.5)	37	2	-	-	26	-	10		VS			
16	I	16 23 45	-24 05 24	a	15± 3	6	46 ± 7	4	4d	14	✳	15.6	:	-	27	-	U	-	[10.4]/7.8	B5	G	11	G	New PMS star
17	I	16 23 45	-24 13 16	a	< 3	2	9 ± 2	6	4d	5.6	1 ?	(17.5)	-	3	-	16	-	-	15.4-17.6	B9V-B8V	C			
																			12		VS			
18	I	16 24 03	-24 35 40	a	< 5	6	18 ± 4	2	17m	5.0	2?(Δm=1)	(17.5)	:	:	-	:	-	-						
19	I	16 24 08	-24 03 16	a	< 5	6	9 ± 4	4	2d	5.1	1	(18.5)	:	-	-	-	-	-						
20	I	16 24 13	-24 45 00	c	< 10	2	262 ±22	C	3h	17	✳✳(Δm=2)	(14.0)	:	:	-	:	-	-		M	G	6.2	G	ROX20-1 pair of new
																				M	G	5.5	G	ROX20-2 PMS stars;
																								superflare?
21	I	16 24 19	-24 34 28	a	< 8	1	54 ± 6	5	2d	14	SR12	13.1v	:	:	-	:	-	-	0.35	M1	CK	4	R	T Tauri
	H	16 24 17.8	-24 34 58.9	-																				
22	I	16 24 20	-24 22 12	a	4± 2	6	16 ± 4	4	1d	6.1	-	-	:	26	-	-	-	OPH12	25		VS			OPHB
23	I	16 24 23	-24 10 52	a	3± 2	2	13 ± 3	5	2d	5.8	-	-	:	22	-	-	-	-	14		VS			
24	I	16 24 29	-24 17 48	a	4± 2	6	9 ± 3	1	23m	3.8	-	-	:	-	-	-	-	-						
25	I	16 24 31	-24 34 38	a	< 5	6	9 ± 2	2	6m	3.5	⊡ ?	(18.5)	:	:	-	:	-	-						
26	I	16 24 32	-24 33 16	a	< 5	6	14± 3	2	2d	5.0	-	-	:	:	-	:	-	-						

TABLE 1—*Continued*

ROX #	det	α(1950) h m s	δ(1950) ° ' "	IPC pos. class	min counts ($10^{-3}s^{-1}$)	obs #	max. counts ($10^{-3}s^{-1}$)	obs #	Δt min	σ comb	optical id. list or PSS	m	near IR id. GSS	VS	VSS	C	E	Radio cont.	A_V	Spectral type	Hα EW (Å)	Ref	Remarks
(1)	(2)	(3)		(4)	(5)	(6)	(7)	(8)	(9)	(10)	(11)		(12)	(13)	(14)	(15)	(16)	(17)	(18)	(19)	(20)	(21)	(22)	(23)	(24)
27	I	16 24 38	-24 32 12	a	< 5	6	8± 3	3	17m	3.8	2	(17.0)	:	:	-	:	-	-							
28	I	16 24 39	-23 57 40	c	6±2	5	12± 3	2	6m	5.7	2	(17.0)	:	:	-	:	-	-							
29	I	16 24 39	-24 15 24	a	18±3	6	50± 6	1	3d	15	SR9=DoAr34	11.4v	:	-	-	-	34	-	0.90	K7	CK	12	CK	T Tauri	
	H	16 24 38.9	-24 15 24.8	-								11.9										6	R		
																						12	G		
30	I	16 24 40	-23 52 52	c	<11	2	27± 5	6	2d	7.3	DoAr33 +2	(15.0) (17.0)	:	:	-	:	U	-				Y	DoAr	(edge of central field)
31	I	16 24 51	-24 33 55	a	< 5	6	22± 4	5	2d	7.2	⊡	(15.0)	:	:	-	:	-	-							
32	I	16 25 11	-24 43 48	b	< 9	A	24± 5	B	(17m)	4.3	⊡+3(Δm=2.5)	(16.0)	:	:	-	:	-	:							
33	I	16 25 32	-24 15 46	a	7±2	6	97±10	4	1d	12	SR20=DoAr38	14.2	:	:	-	:	U	:		< K7	R	16	R	T Tauri	
34	I	16 25 44	-24 21 22	c	6±2	5	13± 4	2	17m	5.4	SR13=DoAr40	13.1v	:	:	-	:	-	:	0.0	M1.5	CK	42	R	T Tauri	
35	I	16 26 32	-24 49 35	b	11±5	A	20± 6	B	(17m)	4.3	⊡+ 2	(12.0)	:	:	-	:	-	:							
36	I	16 26 50	-24 52 34	b	8±4	A	16± 6	B	"	3.8	SA0184424	8.2	:	:	-	:	-	:		A2					
37	I	16 27 08	-25 00 11	b	<10	A	18± 5	B	"	3.6	SA0184429	4.9	:	:	-	:	-	:		B3				Field star ?	
38	I	16 27 19	-25 30 00	b	< 8	B	20± 5	A	"	4.3	⊡ + 5	(15.0)	:	:	-	:	-	:							
39	I	16 27 35	-24 28 04	b	20±5	B	41± 5	A	"	8.6	⊡ + 1	(12.5)	:	:	-	:	U	:							
40	I	16 27 49	-24 05 40	c	6±3	B	13± 4	A	"	3.5	⊡ + 3	(11.0)	:	:	-	:	-	:						Field star ?	
41	I	16 27 50	-24 43 40	b	< 4	A	14± 4	B	"	3.8	8 (Δm=2)	(16.5)	:	:	-	:	-	:							
42	I	16 28 12	-24 27 48	b	39±6	A	44± 6	B	"	10	⊡ + 3	(12.0)	:	:	-	:	U	:							
43	I	16 28 17	-24 23 40	b	56±6	B	71± 7	A	"	13	⊡ + 6	(9.5)	:	:	49	:	-	:						Field star ?	
44	I	16 28 30	-24 21 48	b	7±3	B	17± 4	A	"	5.2	H1-16=DoAr44	12.5v	:	:	-	:	-	:	1.2	K3	CK	59	CK	T Tauri	
45	I	16 28 44	-25 23 16	b	< 8	A	17± 5	B	"	3.6	⊡ + 5	(13.5)	:	:	-	:	-	:							
46	I	16 28 48	-24 49 32	b	13±3	B	18± 4	A	"	4.1	-	-	:	:	-	:	U	:							
47	I	16 29 09	-24 33 55	b	21±6	B	43± 6	A	"	8.1	DoAr51	13.5v	:	:	62	:	U	:		M1	R	7	R		

Explanation of Columns

(1) Rho Oph X-ray source reference number. (2) *Einstein* detector: I = IPC, H = HRI. (4) IPC position class: a = 30″, b = 40″, c = 45″ (error box radius). (6) Reference number of the observation in which the minimum corrected count rate of col. (5) has been found. Observations 1–6 refer to the central field (I3749, I8374, I9541, I9542, I9543); A refers to the first series of observations in the adjacent fields (I3828 to I3831), B to the second series (I8375 to I8378), C to field I8376 only. (8) Same as col. (6), for the maximum count rate. (9) Time interval in which the largest count rate variation has been observed, including upper limits; m = months, d = days, h = hours. (10) Combined statistical significance. (11) Possible optical identifications. *References*: SR = Struve and Rudkjøbing 1949, DoAr = Dolidze and Arakelyan 1959, SAO = SAO catalog, H = Herbig and Rao 1972. *Counterparts on the PSS red print*: * = on the nominal position of the ROX source; ⊡ = only one bright source in the IPC error box; ⊡ + *n* = *n* less bright stars, within the magnitude interval Δ*m* from the brightest; – = no visible counterpart. (12) Magnitude (visible or photographic); suffix v if variable. In parentheses: our own estimate from the PSS red print (accurate to ±0.5 mag). (13)–(17): Possible near-IR counterparts. Numbers refer to the following *lists*: GSS = Grasdalen *et al.* 1973; VS = Vrba *et al.* 1975; VSS = Vrba *et al.* 1976; C = Chini *et al.* 1976; E = Elias 1978. U = Elias (unpublished); – = source undetected; : = source not in the field of view. (18) Radio continuum sources, Falgarone and Gilmore 1981. (19) Visual absorption, in magnitudes (between brackets if from IR data). The figure depends on the spectrum of col. (20). (20) Spectral type; ref. in col. (21). (21) *References*: C, E, VS, see cols. (13)–(17). CK = Cohen and Kuhi 1979; FG = Falgarnoe and Gilmore 1981; R = Rydgren 1980. (22) Equivalent width of the Hα emission line, according to ref. in col. (23) (G = measured by Grindlay after X-ray detection; Y = detected, but EW not available).

TABLE 2

RHO OPHIUCHI CENTER FIELD: CANDIDATE SOURCES ($2 < \sigma < 3.5$)

Source	det	α(1950) h	m	s	δ(1950) °	'	"	optical ident. list or PSS	m	near IR ident. GSS	VS	VSS	C	E	Radio cont.	A_V	Spectral type	Ref.	$H\alpha$ EW(Å)	Ref.	Remarks
(1)	(2)	(3)			(4)			(5)	(6)	(7)	(8)	(9)	(10)	(11)	(12)	(13)	(14)	(15)	(16)	(17)	(18)
C 1	I	16	23	06	-24	20	51	-	-	24	-	-	-	-	-						Source 1 of Lada and Wilking(1980)
C 2	I	16	23	14	-24	20	52	-	-	-	1	-	12	-	-	18 22	B7V-B8V	C VS			
C 3	I	16	23	24	-24	35	56	Do Ar 25	(14.5)	:	:	25	:	-	-						
C 4	I	16	23	25	-24	13	54	-	-	-	-	-	-	-	-						
C 5	I	16	23	26	-24	09	32	1	(17.5)	:	-	-	-	24	-						
C 6	I	16	23	27	-24	18	12	1	(17.5)	32	-	-	-	23	-						
C 7	I	16	23	35	-24	07	00	-	-	:	-	-	-	-	-						
C 8	I	16	23	36	-24	31	56	-	-	:	:	-	:	-	-						
	H	16	23	39.2	-24	31	00.0														
C 9	I	16	23	43	-24	09	32	-	-	38	11	-	-	-	-	16		VS			
C10	I	16	23	44	-24	35	56	⊡+ 1	(18.0)	:	:	-	:	-	-						
	H	16	23	45.3	-24	38	01.0														
C11	I	16	23	55	-24	18	57	-	-	-	5	-	-	-	OPH6?	21		VS			
	H	16	23	54.3	-24	20	20.5														
C12	I	16	23	54	-24	15	40	-	-	40	6	-	-	-	-	20		VS			
																	B9	VSS			
C13	I	16	23	58	-24	38	20	SR24/DoAr29	15.1	:	:	-	:	28	-	3.1/4.5	K2/M0.5	CK	76/24	CK	T Tauri pair
C14	I	16	24	07	-24	12	28	SR21	(13.5)	:	23	31	19	30	-	9 9	B7V	C VS	-		
C15	I	16	24	08	-24	32	20	-	-	:	:	-	:	29	-						
C16	I	16	24	15	-24	31	24	-	-	:	:	-	:	-	-						
C17	I	16	24	17	-24	14	20	-	-	:	-	-	-	-	-						
C18	I	16	24	17	-24	37	16	-	-	:	:	-	:	-	-						
C19	I	16	24	28	-24	29	56	-	-	:	-	-	-	-	-						
C20	I	16	24	37	-24	30	04	⊡	(18.5)	:	:	-	:	-	-						

NOTE.—This table is similar to Table 1, except for the absence of min. and max. corrected count rates (the statistics are too low) and for the IPC position class (*c* for all sources). The count rates are on the order of 5×10^{-3} s^{-1}.

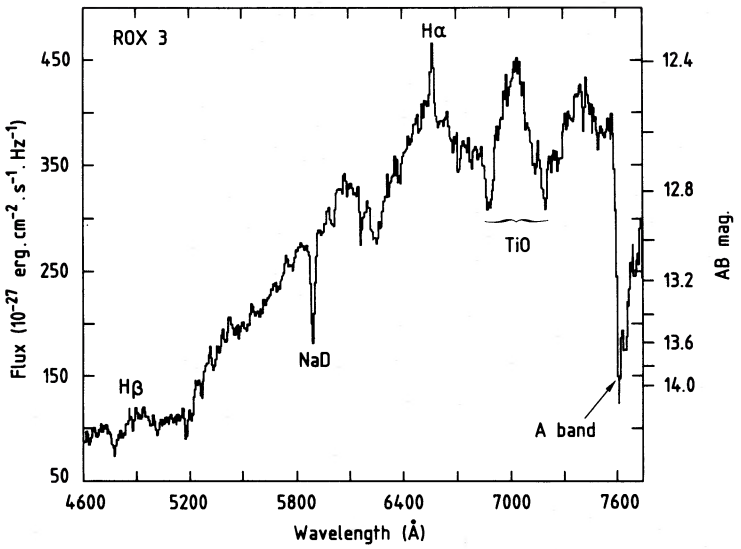

FIG. 4.—Optical spectrum of the previously unknown stellar counterpart to ROX-3. Several emission and absorption features (shown) are typical of late-type pre-main-sequence stars.

part, if any, of 2CG 353+16 may still be a different type of object (for instance, a background quasar; see the case of 2CG 135+01, Pollock *et al.* 1981).

d) *Absorption*

We summarize here a number of salient features which are common to most ROX sources. As indicated by a general deficiency in low-energy photons after removal of the background ($\sim$70% of the sources have a strong maximum near $\sim$1 keV), most sources have a high absorption column density $N_{H,x}$ along the line of sight. The absorption, however, cannot be known reliably when the number of counts in the total IPC passband ($\sim$0.2–0.4 keV) falls below about 40. Above this, the value of $N_{H,x}$, can be estimated if one assumes a spectrum, but the uncertainty on spectral parameters, hence on $N_{H,x}$ becomes reasonably low only above $\sim$100 counts. (The signal-to-noise ratio cannot be improved by merging the images, because the gain and the fluxes are different in each image.) Although various kinds of spectra may be assumed, we have chosen thermal spectra, in accordance with our interpretation (§ IV*c*); most sources have then $kT \approx 0.5$–2 keV. As a result, whenever $N_{H,x}$ can be determined, we find $N_{H,x} \sim$ several 10^{21}–10^{22} cm^{-2}. This is in fact within a factor 2 to 5 of the values deduced from visual extinction, when available (see Table 1).

Because of the impossibility of having good spectral fits below 40 counts, the conversion from counts to flux in the total IPC passband has to be estimated indirectly. For sources detected with more than 100 counts, taking into account the various column densities and temperatures actually deduced from spectral fits and including the uncertainties introduced by possible unknown gain variations (§ I*b*), we find 1 count s$^{-1} \approx (3.3 \pm 0.5) \times 10^{-11}$ ergs cm^{-2} s^{-1}. Between 40 and 100 detected counts, spectral fits are poorer, and the uncertainties correspondingly larger: 1 count s$^{-1} \approx (3 \pm 1) \times 10^{-11}$ ergs cm^{-2} s^{-1}. If we fold through the IPC response a thermal spectrum with $kT = 1$ keV, $N_H = 3 \times 10^{21}$ cm^{-2} (quite typical of the ROX sources detected above 40 counts), we find 1 count s$^{-1} = 3 \times 10^{-11}$ ergs cm^{-2} s^{-1}. Therefore, for the sources detected below 40 counts, we take this value as a good estimate of the conversion factor, in view of the wide similarity between the ROX sources. One then finds for X-ray sources lying at the distance of the cloud ($\sim$160 pc):

$$10^{-3} \text{ counts s}^{-1} = 9 \times 10^{28} \text{ ergs s}^{-1}, \quad (3.1)$$

so that apparent luminosities of the ROX sources are in the range $\sim(0.5\text{–}25) \times 10^{30}$ ergs s^{-1} (see § VII*a*).

IV. TIME VARIABILITY

a) *Time Scales*

As previously discussed, all count rate variations larger than the statistical uncertainties must be real. Now what we observe (see Figs. 1 and 3) is the *apparent* luminosity; because of the uncertainties in the spectra, it is often difficult to derive the *intrinsic* luminosity. However, for a given source, their relative variations should be identical: we checked whether luminosity variations could be caused by fluctuations in absorption by studying hard/soft flux ratios, and no variation can be seen beyond the large error bars (a factor of $\sim$2 for sources with $\gtrsim$40 counts and up to 10 for weaker sources).

We cannot show here all the individual light curves corresponding to Figure 1. Suffice it to say that strong variations (up to a factor of $\gtrsim$10) are detected in several sources, down to within 1 day (see Table 1), i.e., between observation 3 and 4. This is most readily visible when cycling observations 1–6, which make the cloud look like an X-ray Christmas tree. Even the variations observed

at longer time intervals may reflect similarly short time scales. One source, 20 in Table 1, has been observed at even shorter intervals (a few hours) and shows the strongest variability of all ROX sources (see § V*b* below).

b) Distribution of the Flux Variations

The similarity of the spectra and light curves of the ROX sources leads us to assume that the detected sources are statistically independent and of the same nature (at least in X-rays). In other words, we assume that all the sources belong to one single type of X-ray object, seen in different states, which we seek to define. We take into account only the positive detections, and we assume further that the "ground state" is the state corresponding to the lowest energy detected. These are admittedly crude approximations, but they are found *a posteriori* to be probably valid for most ROX sources.

It is then possible to draw a histogram $\mathcal{N}(F_X)$ of the normalized amplitude distribution of the fluxes (F_X = flux in observation i for *any* source normalized by the minimum flux detected for that source). This histogram (Fig. 5) is derived from 86 points = Σ (number of sources) × (number of positive detections above ground state), which we assume is statistically equivalent to one single source observed 86 times. It is remarkable that $\mathcal{N}(F_X)$ may be approximated by a power law for the lower values of F_X (where the statistics are good):

$$\mathcal{N}(F_X) \propto F_X^{-1.4\pm0.2} . \quad (4.1)$$

This law is compatible even with large values of F_X (up to 15), in spite of a few gaps, which probably reflect only the poorer statistics beyond $F_X = 3$.

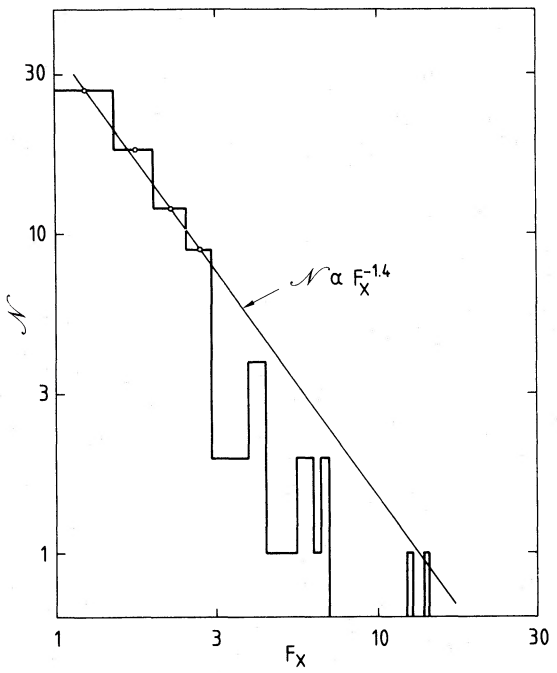

FIG. 5.—Histogram of the amplitude distribution of flux variations $\mathcal{N}(F_X)$ for all ROX sources (see text, § IV*b*). The increment of F_X is $\Delta F_X = 0.5$. F_X = (flux detected in one observation)/(minimum flux detected).

c) Possible Interpretation of the Flux Variations

We wish now to suggest that the observed flux variations may be interpreted in terms of *strong stellar flares*, which *dominate* the X-ray activity of the underlying stars, on the basis of the following arguments.

1. The exponent of the power law found in equation (4.1) is similar to that found by Drake (1971), 1.44 ± 0.01, for the time-integrated flux of solar X-ray flares. This similarity can be explained if all the detected ROX "flares" have durations of the same order (*e*-folding time of 1–2 hours in the case of ROX-20; see below, § VI*a*).

2. Equation (4.1) is reminiscent of the amplitude distribution found by Kunkel (1973) for flares in dMe stars. The distribution is exponential in U magnitude, which can be translated to a power-law distribution $\mathcal{N}(F_U)$:

$$\mathcal{N}(F_U) \propto F_U^{-1.09\pm0.05} . \quad (4.2)$$

In equation (4.2), only the flare luminosity in the U band is taken into account, whereas in equation (4.1), the total X-ray luminosity is used, but this is also essentially the flare luminosity in X-rays. The exponents are not very different. Such a power-law behavior for flares may be explained in terms of a stochastic relaxation phenomenon (Rosner and Vaiana 1978; see also Kuan 1976).

3. While the overall observed light curve does not differ significantly from that of the other ROX sources, this explanation also accounts for several rises in luminosity observed in source ROX-20 (with the amplitude F_X reaching 25).

This is shown by the following detailed study.

V. OBSERVATIONS OF SOURCE ROX-20

a) Identification

As mentioned before (§ I*a*), the ROX sources were found in a mosaic of five IPC fields covering the *COS B* error box with the "middle" field overlapping the four other, mutually adjacent, fields. The source 20 in the list of Table 1 was found in one of the overlapping areas. It was thus observed eight times: twice in the "middle" field, in addition to six times in the "center" field (Fig. 6), at time intervals down to a few hours.

The conspicuous optical counterpart on the PSS red print is an apparent visual binary, with $m_R \approx 14$ and 16 (Fig. 7 [Plate 4]), located at $\alpha(1950) = 16^h24^m13^s.1$, $\delta(1950) = -04°45'0''$. It is the only object visible within the $\sim 30''$ radius IPC error boxes, one for the "middle" field, one for the "center" field (their centers are $\sim 18''$ apart). This star has never attracted the attention of astronomers before. It has not been detected in previous surveys, i.e., Hα, optical, near-infrared, or radio continuum (for references, see Table 1). It was also not reported in our own preliminary investigation (Montmerle, Koch-Miramond, and Grindlay 1981*a*, *b*).

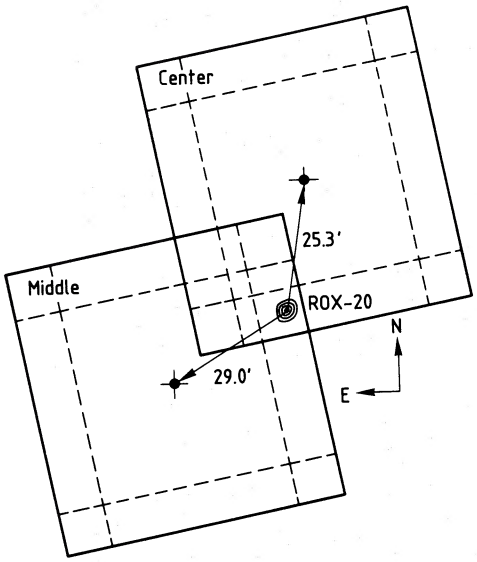

FIG. 6.—Relative positions of two of the five IPC fields observed several times with the *Einstein Observatory* in the region of the ρ Oph dark cloud. The "center" field corresponds to the densest part of the cloud (axis at $\alpha = 16^h23^m58^s$, $\delta = -24°19'52''$). The "middle" field corresponds to the region in the middle of 2CG 353+16 (axis at $\alpha = 16^h26^m$, $\delta = -25°$; see also Figs. 3*a* and 3*b*) and partially overlaps from neighboring IPC fields. The position of the source ROX-20 is indicated, as well as the IPC ribs in each field.

On a Palomar Sky Survey red print, it appears to be lying near the southern edge of a dense part of the ρ Oph cloud (Fig. 7), like many other sources we have detected in the "center" field (Fig. 2).

Spectra of both components of the apparent visual binary were obtained by one of us (J. E. G.) in 1982 June at the Whipple Observatory, Mount Hopkins. Both stars appear to be late-type pre–main-sequence stars with weak Hα emission. The spectra are rather similar to that shown in Figure 4 and do not allow an obvious choice to be made as to which component gave rise to the X-ray flare.

b) Light Curve

In the "center" fields, the source ROX-20 was analyzed by taking source counts in a circle of radius 2'.7, and the background in an annulus of radii 2'.7 and 6'.7. In the "middle" fields, the counts were taken in a circle of radius 3'.3, and the background in an off-centered circle, 7'.2 away, of the same radius.

Using the nominal vignetting corrections, we find the light curve of Figure 8, which spans nearly 2 years (additional details may be found in Table 3). Two strong luminosity variations (factor $\gtrsim 10$) are seen, on time scales of a few hours. Of particular interest is the event beginning on 1981 February 7, i.e., observations 4, 5, and 6. After (presumably) an unseen rise, the luminosity decreased by a factor of 5 in less than 3 hours, and by a factor of more than 25 in 27 hours. Two days later, the luminosity had risen again, then returned to about the same value 2 days later still.

Now the validity of the data leading to this rather spectacular behavior could *a priori* be affected by some problems.

First, in both the "center" and "middle" fields, ROX-20 is extremely off-centered, being even *beyond* the ribs (Fig. 6), where corrections are not well known. However, the respective positions with respect to the axis are about the same ("center" field: 25'.3; "middle" field: 29'.0); hence the vignetting corrections must be of the same order (nominally 1.6 and 2.2, respectively) and should not affect much the relative luminosities.

Second, as mentioned previously (§ II*b*), more than 4' away from the axis, the gain of the IPC is not known precisely (Gorenstein, Harnden, and Fabricant 1981). This is particularly critical for ROX-20 since it lies far

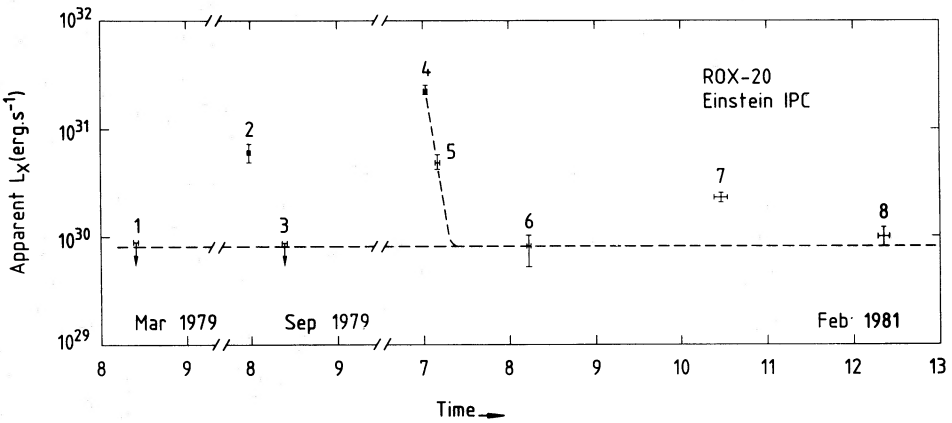

FIG. 8.—Light curve of ROX-20, based on the eight observations of this source obtained between 1979 and 1981. Numbers refer to the observations (see Table 3). The dotted horizontal line is a possible quiescent flux from the source; the dotted line at observations 4 and 5 is an exponential fit to the decrease in intensity, which we interpret as the cooling phase of a very strong stellar flare. We note that the data is compatible with a similar interpretation for observations 2 and 7. The ordinate is the *apparent* luminosity of the source; because of absorption along the line of sight, the *intrinsic* luminosity should be approximately 5 times larger (see Table 3).

TABLE 3

OBSERVATIONAL DATA ON SOURCE ROX-20

Variable	Obs. 1 I3749.1[a,b] C[c]	Obs. 2 I3829[a] M[c]	Obs. 3 I3749.2[a] C[c]	Obs. 4 I8276[a] M[c]	Obs. 5 I8374[a] C[c]	Obs. 6 I9541[a] C[c]	Obs. 7 I9542[a] C[c]	Obs. 8 I9543[a] C[c]
Date (begin)	1979 Mar 8	1979 Sep 7	1979 Sep 8	1981 Feb 7	1981 Feb 7	1981 Feb 8	1981 Feb 10	1981 Feb 12
Hour (UT) begin	0933:10	2326:17	0854:56	0132:24	0424:26	0521:31	0856:03	0639:41
Hour (UT) end	1009:21	0006:33	0933:51	0201:45	0509:29	0604:31	1355:03	0956:58
Exposure (s)	1979.2	1247.0	2141.8	1646.4	2004.2	1688.0	2881.9	3509.1
Raw counts (bins 3–13)	<10.0[d]	38.1 ± 6.8	<10	193 ± 16.3	71.0 ± 9.7	9.5 ± 4.0	48.9 ± 7.8	24.3 ± 6.3
Corrected count rate ($\times 10^{-3}$ s^{-1})	<10.6	68.5 ± 12.3	<9.7	262 ± 22.2	56.6 ± 7.8	9.0 ± 3.8	27.2 ± 3.5	11.0 ± 2.7
L_x($\times 10^{30}$ ergs s^{-1})[e]	<4.5	30.0 ± 5.5	<4.5	114 ± 9.5	24.5 ± 3.5	4.0 ± 1.5	12.0 ± 1.5	5.0 ± 1.0

[a] Field location.
[b] We designate the two observations merged in field I3749 by I3749.1 and I3749.2.
[c] M = middle field; C = center field (see Fig. 6).
[d] 2 σ upper limits.
[e] Intrinsic luminosity, with an absorption factor $\alpha = 5$, and with 10^{-3} counts s^{-1} = 9×10^{28} ergs s^{-1} at 160 pc.

from the observation axes, and because, in the case of repeated observations, the actual gain may differ in an unknown way from the nominal gain between neighboring pixels and between observations. However, the observed spectrum of ROX-20, taken for instance at maximum observed luminosity (Fig. 9) shows that the low-energy channels (<1 keV) are strongly cut off. Because of this, the total number of counts, and hence the observed flux in the IPC passband, is essentially insensitive to differences between nominal and actual IPC gains (as was the case of most ROX sources; see § II*b*).

Therefore, only the *absolute* values of the count rates may be affected (because of possible deviations from the nominal vignetting corrections, or unknown systematic errors) but not their *relative* values. Hence, we conclude that the observed count rate variations (i.e., flux variations) are real, the associated errors being only the standard statistical errors. We will now discuss further the 1981 February 7 event.

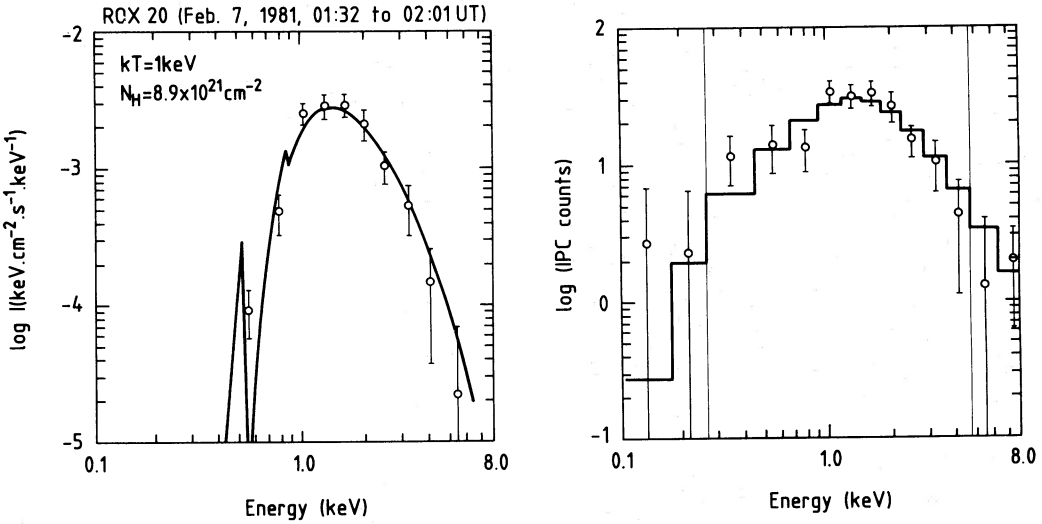

FIG. 9.—Spectrum of source ROX-20 at its maximum observed intensity (field I8376, observation 4). *Left*: incident spectrum; *right*: observed spectrum. The fit with a thermal spectrum (here $kT = 1$ keV) and $N_H = 8.9 \times 10^{21}$ cm^{-2} has been found *excluding* the two first, and two last channels (*thin vertical lines*): $\chi_{min}^2 = 6.8$. Other spectra (even nonthermal) may, however, provide fits only slightly less good than this kind of spectrum, because the total number of raw counts (here, 193 ± 16 after background removal) is not sufficient to make a significant difference between various incident spectra.

VI. ANALYSIS OF THE 1981 FEBRUARY 7 EVENT

a) *Time Variation*

First, we note that the time scale for the decrease in luminosity between observations 4 and 5 is of the same order than the *e*-folding times of the decrease of large solar flares (e.g., Moore *et al.* 1980). Assuming that we are indeed in the presence of a flare (see § IV*c*), the apparent luminosity of ROX-20, L_x', can be split into a "quiescent" (coronal ?) component $L_{x,Q}'$, and a "flare" component $L_{x,F}'$. At any given time t,

$$L_x'(t) = L_{x,Q}' + L_{x,F}'(t) . \quad (6.1)$$

For observations 4, 5 and 6 (Table 3), we find a possible representation of the form

$$L_x'(10^{30} \text{ ergs s}^{-1}) = 0.8 + 22.2 \exp [-t(\text{hr})/1.75] \quad (6.2)$$

with $t = 0$ in the middle of observation 4, and $t \geq t_m$, unknown time of the flare maximum. It is reasonable to consider that $L_{x,Q}' = 0.8 \times 10^{30}$ ergs s^{-1} *is* indeed a quiescent state, since it is compatible with observations 1 and 3 (which give $L_x' < 0.9 \times 10^{30}$ ergs s^{-1}), and 8 ($L_x' = 1.0 \pm 0.2 \times 10^{30}$ ergs s^{-1}), as shown on Figure 8 (see also Table 3).

Now it is possible to check whether equation (6.2) is also compatible with the count rate measured *within* the $\sim$1600 s duration of observation 4. The count rate variation between the beginning and the end of that observation, expected on the basis of equation (6.2), is $\sim$0.020 counts s^{-1} per 1000 s, corresponding to a $\sim 1.4\,\sigma$ deviation in the observed average count rate (Table 3). Such a deviation is obviously unobservable against the normal statistical fluctuations, and indeed no variation was detected within observation 4 (see also § VII*c*).

b) *Spectrum and Energy Content*

At maximum, the best ${\chi_m}^2$ fit to the observed spectrum (removing the extreme channels 1–2 and 14–15 as being dominated by background) gives an absorption column density $N_{\text{H},x} = 10^{22}$ cm^{-2}, with a thermal spectrum characterized by $kT = 2$ keV. Writing the *intrinsic* luminosity $L_x = \alpha L_x'$, one finds, with such a spectrum

$$\alpha \approx 5 . \quad (6.3)$$

(This figure, however, is rather uncertain since other spectra, even nonthermal, may give fits nearly as good with respect to a ${\chi_m}^2$ test.)

From (6.2), the intrinsic luminosity of the event is then

$$L_x(10^{30} \text{ ergs s}^{-1}) \approx 4.0 + 100 \exp [-t(\text{hr})/1.75] , \quad (6.4)$$

provided that $N_{\text{H},x}$ does not change during the flare decrease, i.e., is dominated by interstellar absorption. This is a reasonable hypothesis in view of the high value of $N_{\text{H},x}$ and of the location of ROX-20 with respect to the cloud (Fig. 7). The energy of the flare in X-rays, $E_{x,F} = \int_{t_m}^{\infty} L_{x,F}\,dt$, is readily computed to be (from the beginning of observation 4) at least

$$E_{x,F} \geq 8 \times 10^{35} \text{ ergs} . \quad (6.5)$$

This is almost two orders of magnitude larger than the energy detected in the flare of the T Tauri star DG Tau by Feigelson and De Campli (1981), $\sim 10^{34}$ ergs. (This figure is really a lower limit to the actual energy, since only the rise phase of that flare was observed.) Therefore, the 1981 February 7 event observed in ROX-20 appears as perhaps the most powerful stellar flare ever recorded (see § VII*b* for further discussion).

c) *Physical Parameters of the Plasma*

Assume now that the observed decrease is due simply to flare *cooling*, after an unobserved phase of energy input. From equation (6.4), the characteristic cooling time t_c is

$$t_c = 1.75 \text{ hr} . \quad (6.6)$$

In solar flares, two cooling mechanisms compete: radiative cooling and conductive cooling. Usually, radiative cooling is thought to dominate, especially in large flares, but conductive cooling may also be important (Moore *et al.* 1980; see also, e.g., Gabriel, *et al.* 1981). On the Sun, flares are thought to occur from magnetic reconnection (Priest 1981), and we suspect this is the case here. The corresponding characteristic times are

$$t_{c,\text{rad}} = 3kT/[n_e P(T)] \text{ (radiative)} \quad (6.7)$$

$$t_{c,\text{cond}} = 3k\beta n_e l^2/\kappa(T) \text{ (conductive)} . \quad (6.8)$$

In these expressions, the X-ray emitting plasma has a density n_e, a temperature T, and a typical size l. $P(T)$ is the radiative cooling function, $P(T) \approx 2 \times 10^{-23}$ ergs cm^3 s^{-1} around 10^7 K (within a factor of 2, depending on the authors; see, e.g., McWhirter, Thonemann, and Wilson 1975; Raymond, Cox, and Smith 1976; Raymond 1979); $\kappa(T)$ is the thermal conductivity, $\kappa(T) = 10^{-6} T^{5/2}$ ergs s^{-1} K^{-1} cm^{-1}. The factor β takes into account the influence of geometrical factors on the transport of electrons out of the X-ray emitting region: if one assumes, in analogy with the solar case, that the plasma is contained in one or several arches, then $\beta \approx 5$–10 (Moore *et al.* 1980; Antiochos and Sturrock 1976).

Now, from Feigelson and De Campli (1981) (for instance), the emission measure EM at maximum (observation 4; $T = 1$–2 keV) is computed to be

$$\text{EM} \approx (0.6\text{–}1.2) \times 10^{55} \text{ cm}^{-3} . \quad (6.9)$$

With EM defined by

$$\text{EM} \sim (4\pi/3) {n_e}^2 l^3 \quad (6.10)$$

and from equations (6.7) and (6.8), one finds a critical density n_c such that $t_{c,\text{rad}} = t_{c,\text{cond}}$

$$n_c = 5 \times 10^{25} T^{21/4} \beta^{-3/2} \text{ EM}^{-1} \text{ cm}^{-3} . \quad (6.11)$$

Thus, when $n_e > n_c \approx 2 \times 10^6$ cm^{-3}, radiative cooling dominates. From equation (6.7), the plasma density corresponding to the radiative cooling is

$$n_e(10^{11} \text{ cm}^{-3}) = 0.6T(10^7 \text{ K})/t_c(\text{hr}) , \quad (6.12)$$

i.e., $n_e \approx 3$–6×10^{10} cm^{-3}. Hence, radiative cooling is by far the dominant cooling mechanism. This density is, remarkably, on the low side of the densities typical of large solar flares.

In addition, from equation (6.10), one can estimate the typical size of the X-ray emitting plasma

$$l(10^{10}\text{ cm}) = 1.5 L_x(10^{30}\text{ ergs s}^{-1})^{1/3} \times t_c(\text{hr})^{2/3} T(10^7\text{ K})^{-1/3}\ . \quad (6.13)$$

For ROX-20, the observed maximum corresponds to $l \gtrsim 10^{11}$ cm. This is about one order of magnitude larger than the largest solar flares and than flares on dMe stars or other ROX sources (see below). In fact, this size is the main factor explaining the increase in luminosity (or emission measure), $\sim 10^5$ times with respect to the largest (class 3) solar flares. If ROX-20 is a T Tauri star of typical radius $R_* \approx 2$–$3\ R_\odot$ (see, e.g., De Campli 1981; also Cohen, Bieging, and Schwartz 1982), one has $l \approx 0.5$–$0.7\ R_*$, impressive enough, perhaps, to speak of a "superflare."

VII. DISCUSSION AND IMPLICATIONS

a) Energetics of Flares from ROX Sources

The preceding sections have shown that an interpretation of the time variability in terms of flares in ROX sources is quite plausible, and requires very few assumptions. If this is indeed the case, this flaring activity *dominates* the X-ray emission. Hence, it is *a priori* difficult to define a "typical" ROX luminosity. Quantitative estimates may, however, be obtained in two ways: by taking a *space* average $\langle L_x \rangle_s$, i.e., dividing the total luminosity in IPC exposures by the number of sources detected, and by taking a *time* average $\langle L_x \rangle_t$, for a given source, by dividing the total counts observed by the total effective exposure. When considering all the sources together, the range of $\langle L_x \rangle_t$ gives a measure of the dynamic range of $\langle L_x \rangle_s$. Taking into account an average factor ~ 3.5 representing a mean absorption (weighted according to the values of $N_{\text{H},x}$ over the sources where it can be estimated), the *intrinsic* average ROX luminosities turn out to be:

$$\langle L_x \rangle_s \approx 5 \times 10^{30}\text{ ergs s}^{-1} \quad (7.1)$$

$$\langle L_x \rangle_t \approx 2\text{–}20 \times 10^{30}\text{ ergs s}^{-1}\ . \quad (7.2)$$

These results were obtained for the ROX source in the "center" field, but from Table 1, it can be seen that they are also compatible with the luminosities of the other ROX sources, for which there is less information.

Assuming the flare events have typical durations comparable to that of the flare from ROX-20, the typical flare energies $E_X \approx 10^{34}$ ergs. The typical flare emission regions have size scale $l \approx 1 \times 10^{10}$ cm (cf. eq. [6.13]). Thus if the flares are due to magnetic reconnection, the typical magnetic fields are in the range 100–300 gauss.

Now comparing the flare activity with the underlying, presumably coronal, emission, one has the following results: (1) one flare out of two has an intensity at least twice that of the quiescent value (i.e., $F_x \geq 2$, see § IV*b*), and (2) these flares contain about *half* of the total X-ray energy detected in the cloud

$$L_{x,\text{tot}}(\text{flares with } F_x \geq 2) \approx 0.5 L_{x,\text{tot}} \approx 10^{32}\text{ ergs s}^{-1}\ . \quad (7.3)$$

For individual stars, the average X-ray luminosity is at most a fraction of a percent of the total bolometric stellar luminosity, but in particular cases, like ROX-20, it can reach a few percent. In fact, in X-rays, the ROX-20 "superflare" alone is almost as luminous as the entire cloud.

But is ROX-20 really a peculiar object? Probably not, in view of the power-law flare amplitude distribution discussed in § IV*b*, and its other characteristics which seem, at face value, typical of the other ROX sources. Rather, ROX-20 appears as having been the seat of a particularly strong (but rare) event, belonging only to the tail of the flare amplitude distribution. The flaring mechanism for the event observed on 1981 February 7, must however be quite efficient.

Ongoing optical observations will help in assessing the exact nature of this star.

b) Comparison with Other Flare Phenomena

It is useful to compare the "typical" value of the ROX luminosity, given by equation (7.1) (but bearing in mind the dynamic range given by eq. 7.2), with the corresponding values for other stars displaying X-ray flares. Table 4 gives a comparison of this figure and other derived parameters, for the Sun, several dMe (flare) stars, and PMS-related objects (ROX sources, and the T Tauri star DG Tau).

From Table 4, it can be seen that ROX sources and dMe stars have essentially similar properties, except that the *size* of the ROX flares is somewhat larger (assuming that the cooling time of ROX-20 is typical of all ROX sources). Correspondingly, to a lesser extent—and as is observed on the Sun—the plasma density decreases. This can be expected since on the Sun larger flares tend to occur at higher altitudes with respect to the surface (see Moore *et al.* 1980). Note also that, although more extreme, the flares in DG Tau and ROX-20 follow the same trend—an additional argument in favor of our interpretation. A further matter of comparison is the study of the L_x/L_{opt} ratio (see, e.g., Kahn *et al.* 1979), which gives an insight into the physical mechanism of the flares. The ideal tool, in this respect, is to perform simultaneous X-ray and optical observations. Although such data are unavailable for ROX sources, it can be noted that the results obtained by Worden *et al.* (1981) on optical flares of T Tau stars, if scaled to the duration of the ROX-20 flare, assumed to be typical of the ROX sources, suggest a ratio $L_x/L_{\text{opt}} \sim 1$ on average. This is in the range of what is observed for flare stars (e.g., Haisch *et al.* 1977; Kahn *et al.* 1979). If this proves to be the case, then X-ray heating may be an important contributor to the energy balance in the layers of T Tauri stars and related objects, as it is

TABLE 4

PROPERTIES OF STELLAR X-RAY FLARES AT MAXIMUM

Star		L_x(max) (10^{30} ergs s^{-1})	T (10^7 K)	EM (10^{53} cm^{-3})	E_x (10^{30} ergs)	Size (10^9 cm)	Density (10^{10} cm^{-3})	Reference
Sun	compact flares	$\sim 10^{-4}$	1–2	$\sim 10^{-5}$	10^{-1}	$\sim 10^{-1}$	10–100	1
	flares	$\sim 10^{-3}$	1–2	10^{-5} to 10^{-4}	~ 1	$\gtrsim 1$	10	1
	class 3 flares	$> 10^{-3}$	1–2	$> 10^{-3}$	$\gtrsim 10$	> 10	1–10	1
dMe stars	AD Leo	1.6	(3)	1.4	...	(~3)	(10)	2
	YZ CMi[a]	8	(1)	5	...	...	...	2
	AT Mic	16	3	14	≥ 500	(~7)	(10)	2
	Prox. Cen[b]	1.8	(1)	0.46	...	...	...	3
	UV Cet	2.0	(~1)	1.2	...	...	...	2
T Tau and related stars	ROX[c] sources	~5	2	5	$\lesssim 10^4$	(10–30)	(10–20)	4
	DG Tau	$\gtrsim 20$	(1)	$\gtrsim 10$	$> 10^4$	[50]	[10]	5
	ROX 20	~100	1–2	~100	$\sim 10^6$	~100	3–6	4

NOTE.—Parentheses enclose figures estimated or assumed by the authors; square brackets enclose figures estimated or assumed by us.

[a] For coordinated X-ray, optical, and radio observations of a smaller flare, see Kahler *et al.* 1982.

[b] For the X-ray detection of the quiescent state and observation of a smaller flare, see Haisch *et al.* 1980.

[c] Average properties; see § VII*a* for details.

REFERENCES.—(1) Moore *et al.* 1980. (2) Kahn *et al.* 1979. (3) Haisch *et al.* 1977. (4) This work. (5) Feigelson and De Campli 1981.

for dMe stars (Cram 1982), and may perhaps give a clue to their peculiar structure.

c) *X-Rays from T Tauri Stars*

Restricting the total sample of ROX sources to those identified with known T Tauri stars (Table 1), it is remarkable that they correspond to ~80% of successful detections, whereas ~30% only were seen by previous authors from various samples (Gahm 1980; Feigelson and De Campli 1981; Walter and Kuhi 1981).

The time variability of the ROX sources and our longer overall exposure fully explains this effect. Indeed, in *individual* exposures, we see only between 10% and 50% of the known T Tauri stars; the remainder is obtained by summing up the exposures. This variability supports one conclusion of Gahm (1980) who noted a correlation between the Herbig luminosity class and the positive detection in X-rays (there is no luminosity class available for the ρ Oph T Tauri stars). It is also of course consistent with the count rate variability observed in DG Tau by Feigelson and De Campli (1981) within one observation. Interpreting this variability in terms of flares is also consistent with previous negative results. The reason for this somewhat paradoxical statement is as follows. The exposure times of the previous *Einstein* observations on T Tauri stars were all in the range $T_{\rm exp} \approx 1600$–2500 s (like our own, if taken separately). Compared to this, the flare rise time T_r, such as observed in DG Tau, is only of a few minutes. On the other hand, since the e-folding time for the flare decrease T_d observed in ROX-20 is on the order of a few hours, the time interval between subsequent flares (detectable by *Einstein*) from the same star T_f is presumably at least several T_d, i.e., at least about half a day. Therefore, for a "typical" T Tauri star observation by *Einstein*, one has $T_r \ll T_f$, and $T_d \gg T_{\rm exp}$: it is clear that, *within a random observation*, the probability of detecting a *rising* flare is very small (in fact, it has been 1 in 56 known T Tauri stars observed to date, or 1 in 94 if one includes the ROX sources), and finding evidence for a flare *decrease* is essentially impossible, owing to statistical uncertainties on low count rates, within one observation (see above § VI*a*).

The only way to detect such a flaring activity in X-rays in typical IPC images is by using several repeated exposures of the same region, whereas the previous authors had only sets of single exposures at their disposal. Another way is of course to observe the same region continuously during several days: such observations are planned with the EXOSAT satellite. On the other hand, we note that recent observations of T Tauri stars at UV and optical wavelengths also concur towards the same interpretation. Giampapa *et al.* (1982) find evidence for the existence of extensive regions similar to solar plages (see also Kuan 1976), and Mundt and Giampapa (1982) have detected a rapid time variability in optical line profiles. However, optical observations of coronal lines put very low upper limits to the presence of an X-ray emitting corona (Gahm and Krautter 1982).

In this context, the suggestion by Walter and Kuhi (1981) of the presence of a "smothered corona" to explain the low detection fraction of T Tauri stars in X-rays may have to be revised—unless, of course, the T Tauri stars in ρ Oph are of a very different nature than the stars surveyed by these authors. To illustrate this point, we plot the X-ray luminosity (maximum, minimum, and time-average $\langle L_x \rangle_t$ in the sense defined above, § VII*a*) as a function of the equivalent width EW of the Hα emission line, when known (Fig. 10).

From the Walter and Kuhi data, there was some evidence for an anticorrelation of L_x versus EW (Hα), i.e., for a decrease in L_x accompanying an increase in the size of the "smothering" envelope. This anticorrelation essentially disappears for the ROX sources, although, strictly speaking, some trend remains when one splits the data into two groups, below and above EW(Hα) $\approx$ 20 Å. The situation is obviously complex,

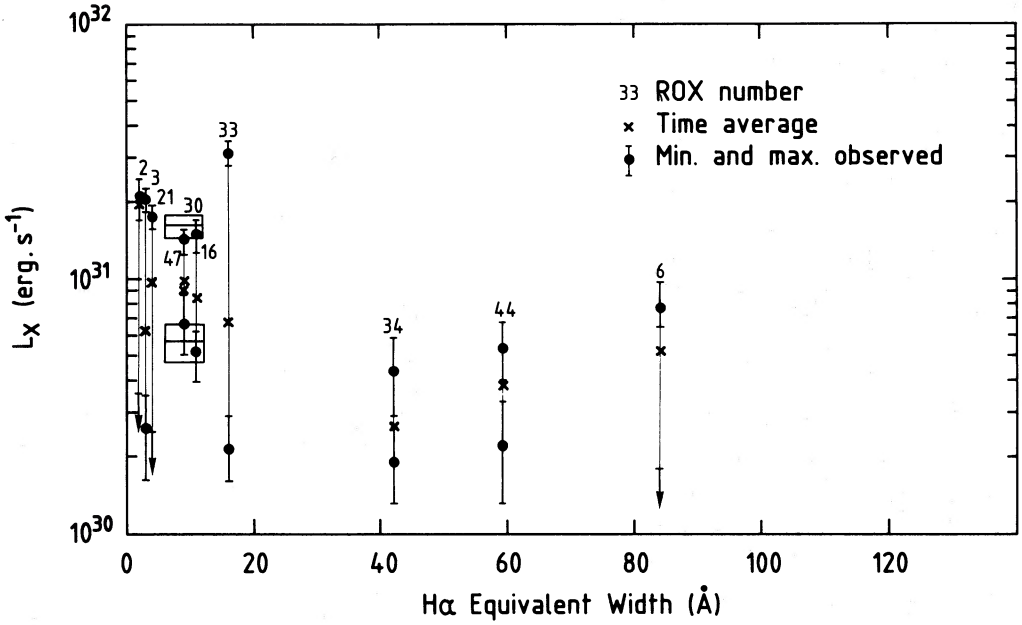

FIG. 10.—A plot of the intrinsic luminosity L_x vs. the equivalent width (EW) of the Hα emission line, for the ROX sources in which it is available (see Table 1). Crosses indicate time averages $\langle L_x \rangle_t$; minimum and maximum detected luminosities are also shown. No observation of time variations in EW(Hα) is available.

and some kind of "smothering" effect cannot be completely excluded.

d) Possible Links between X-Ray Activity and Age

It is possible to broaden somewhat the implications of this flaring activity in T Tauri stars by bringing together several soft X-ray results.

1. A variability of a factor of $\lesssim 2$ has been observed on time scales of days in Cyg OB2 stars 8A and 5 (Vaiana 1981), and on time scales of hours in several stars of the central Orion region (Ku, Righini-Cohen, and Simon 1982).

2. The possible detection of a Herbig-Haro object, HH-1 in Orion, at a level of $\sim 6 \times 10^{30}$ ergs s^{-1}, has been reported (Pravdo and Marshall 1981).

3. The ROX sources associated with early B stars are variable and detected at a level of $\sim$a few 10^{30}–10^{31} ergs s^{-1} (see Table 1). These stars must be very young, since they are embedded in compact H II regions ($\lesssim 10''$ across). Conversely, the B2V star HD 147889, close to ROX-1, is probably much older, since the associated H II region is several arc minutes in size (see Falgarone and Gilmore 1981) and is not detected (HRI data). The corresponding upper limit, $\sim 10^{30}$ ergs s^{-1}, is not incompatible with the *Einstein* data on main-sequence B stars (Vaiana *et al.* 1981).

Therefore, we wish to suggest that the intense flaring activity in the ROX sources is in fact a *general feature of very young stellar objects* whatever their mass or exact evolutionary status. If true, X-rays would be one of the best tools so far to detect them, provided one has the adequate field of view and time coverage.

Going one step further, the X-ray activity, as measured by an "average" luminosity (in the sense defined in § VII*a*) may be linked closely with *rotation.* Indeed, there is already a strong correlation between the X-ray luminosity L_x and rotation ($v \sin i$) in late-type stars, a possible coupling being magnetic fields (Pallavicini *et al.* 1981; Vaiana 1981). This correlation covers four orders of magnitude in L_x, and two orders of magnitude in $v \sin i$; the typical spread of the data points is a factor of 3 in L_x. This spread may include a contribution from flares. However, without some kind of time-dependent observations, this contribution would be hard to single out: more than 80% of the flares are expected to be less than 3 times brighter than the quiescent (coronal) luminosity, if the flares of late-type stars behave like those of the Sun or of ROX sources. On the other hand, links between rotation and X-ray activity are also advocated in the case of close binaries, for which the orbital momentum forces synchronous rotation, for instance in the dMe stars, probably all close binaries. The existence of flare phenomena in the Hyades (Stern 1982) goes along the same lines. Inasmuch as rotation is, in turn, linked with age, the *X-ray activity for single stars or loose binaries would decay with age*, a readily testable suggestion. There is already some preliminary evidence for such a trend (Vaiana 1981).

e) Ionization Balance and Heating of the ρ Oph Cloud

The total intrinsic X-ray luminosity $L_x \approx 2 \times 10^{32}$ ergs s^{-1} (eq. [7.3]), observed within the IPC fields corresponding to the *COS B* error box, may indicate that a significant source of ionization (of the gas) and of heating (of the dust) is present within the cloud, owing to the X-ray emission of embedded PMS objects.

The ionization will affect the molecular chemistry of the cloud. This influence may even be higher in ρ Oph than in Orion (Krolik and Kallman 1983), as can be seen when comparing the corresponding mass for both clouds.

In Orion, the total X-ray luminosity observed within the square degree of the IPC field is $L_x \approx 1.2 \times 10^{33}$ ergs s^{-1} (Ku and Chanan 1979). From Kutner *et al.* (1977), we estimate the corresponding mass, which appears as a condensation in the southern complex, to be $\sim 5 \times 10^4\ M_\odot$. In ρ Oph, L_x is smaller by a factor of 6, whereas the mass of the central region (encompassed by our observations) is $\sim 2 \times 10^3\ M_\odot$ (Encrenaz, Falgarone, and Lucas 1975; see also Myers *et al.* 1978; Pérault and Falgarone 1982). Therefore, the observed X-ray luminosity per unit mass in the IPC fields is comparatively higher in ρ Oph than in Orion by a factor of ~ 4 (for γ-rays, see § VII*f*).

The study of molecules like C_2^+, C_2H^+, CH^+, $C_2H_2^+$, or HCN^+, which are the most sensitive to X-ray photoionization (Krolik and Kallman 1982) would yield valuable information, in particular on various arrays of chemical reactions. This would be in fact easier in ρ Oph, since the cloud is 3 times closer than Orion. On the other hand, in ρ Oph, L_x is much smaller than the bolometric luminosity of the earlier B stars known to be embedded in the cloud or closely associated with it: the three B2V and six B3V stars (Falgarone and Gilmore 1981), altogether supply $L_B \approx 2.5 \times 10^4\ L_\odot$ (see Panagia 1973). This value is only a lower limit to the energy input from stars into the essentially optically thick cloud, since it does not include the contribution from lower mass stars. Even assuming that the unknown contribution of the absorbed X-ray sources presumably present in the $\sim 500\ M_\odot$ core of ρ Oph (Lada and Wilking 1982) is very high, for instance by taking $(L_x/M)_{\rm core} \sim 10$ or 50, L_B is already a factor $\gtrsim 10^5$ larger than L_x. In other words, the contribution of X-rays to heating dust grains will surely be negligible with respect to heating by stars. The thermal balance of the cloud must be assessed from far-IR ($\sim 100\ \mu$m) data, by wide field experiments, like the AGLAÉ balloon experiment (see Boissé *et al.* 1981, and references therein). Such data are now being analyzed (E. Caux and J. L. Puget 1982, private communication).

f) *Possible Links with the Protosolar Nebula and the γ-Ray Source*

The present study has shown that the eruptive phenomena on the suspected PMS object, counterparts to the ROX sources, are essentially solar-like, the differences being only in size (more and more surface phenomena on stars may also be explained in term of solar-like phenomena; see, e.g., the starspots of BY Dra stars). If this is so, then one would expect the X-ray flares to be accompanied by a massive *injection of low-energy particles* (in the MeV range) (e.g., Gorenstein 1981; see also Mullan 1979). Therefore, one can expect observable consequences as regards the irradiation of the protosolar nebula (e.g., Worden *et al.* 1981; Feigelson 1982), and, also, one can perhaps explain the excess γ-ray flux in the ρ Oph cloud, as follows.

1. *Protosolar nebula.* There are large uncertainties in the particle flux derived from a scaling of X-ray flares. Nevertheless, Feigelson (1982) argues that a number of abundance anomalies in meteorites ($^{14}N/^{15}N$, ^{26}Al, etc.) may be accounted for by spallation reactions during the irradiation of the protosolar nebula, by flares ~ 4000 times stronger in the proto-Sun than the most powerful present-day solar flares. This figure is consistent with Hα emission, *U* band photometry, and X-ray observations of PMS stars. From Table 4, one gets an average factor $\lesssim 5000$ for ROX sources, consistent with the above picture. Note that the high level of activity we find for T Tauri stars is also consistent with that required for the proto-Sun to explain the Earth's primordial atmosphere (e.g., Nakazawa and Nakagawa 1981).

2. *Gamma-ray source.* If associated with the ρ Oph cloud, the γ-ray source 2CG 353+16 has a luminosity $L_\gamma \approx 10^{33}$ ergs s^{-1}, i.e., 10 times the energy derived from equation (7.3). Hence, there cannot be a direct connection between the observed X-rays and γ-ray source. However, if the ROX sources are more or less typical PMS objects, then along the lines of Paul, Cassé, and Montmerle (1981), but based on more recent data, one can expect them to have a considerable *mass loss*, with mass loss rate $\sim 10^{-8}\ M_\odot\ yr^{-1}$, terminal velocity ~ 300 km s^{-1} (see Cohen, Bieging, and Schwartz 1982; Bertout and Thum 1982; Felli *et al.* 1982; De Campli 1981), i.e., a mechanical energy of $\sim 3 \times 10^{32}$ ergs s^{-1} each. This mass loss may be driven by Alfvén waves provided the surface magnetic field is of order ~ 100 gauss (De Campli 1981). This value is in fact consistent with our value derived above for the magnetic field in the flare emission regions. If ~ 60 such objects are present in the cloud (assuming that half of the sources of Table 2 are real; see above § III*b*) the overall kinetic "luminosity" L_w is:

$$L_w \approx 2 \times 10^{34} \text{ ergs } s^{-1}, \qquad (7.4)$$

i.e., 20 times L_γ. This figure is in fact a lower limit, because of the possible presence of unseen sources in the core. It could be up to 20 times higher if the nine early B stars embedded in the cloud (Falgarone and Gilmore 1981) lose mass in accordance with their spectral type (see Lamers 1981). Then, winds may provide the necessary energy and acceleration (since MeV particles have to be boosted in the GeV range to induce γ-rays), perhaps at the wind shock boundary (Cassé and Paul 1980; see also Montmerle and Cesarsky 1981). The details of such a model, involving injection by PMS stars, acceleration at the wind boundary, and particle trapping within the cloud, are now under study (T. Montmerle *et al.* 1982, in preparation). We note the various possible difficulties specifically connected with shock acceleration by stellar winds in dense regions (Völk, Morfill, and Forman 1981; Völk and Forman 1982). Finally, it is interesting to note that the γ-ray

luminosity of that part of the Orion cloud which lies within the IPC field of Ku and Chanan (1979), scaled to the relevant mass (§ VII*e*), is 6.1×10^{33} ergs s^{-1} (see Caraveo *et al.* 1980), i.e., 4 times less than the ρ Oph cloud (per unit mass), just as in X-rays.

VIII. CONCLUSIONS

In the course of an extensive guest investigation, both in space and time, of the ρ Oph dark cloud region, with the *Einstein Observatory*, ~ 50 time-variable soft X-ray sources were discovered ("ROX" sources), 20 more being tentative detections. As a class, these sources are most likely pre–main-sequence, or very young objects; this is shown by the spectral information on their stellar counterparts, when available, and by their spatial distribution, closely following that of the cloud material.

We interpret the time variability of these sources as due to a strong and widespread flare activity. If this is the case, and to the extent that PMS (or very young) objects in the ρ Oph cloud are representative of similar objects in general, then X-ray flares appear to be the *dominating* form of surface activity of PMS and very young objects. This is the case, in particular, for T Tauri stars. One of these flares may even have been the largest X-ray stellar flare ever recorded, reaching a luminosity of $\sim 10^{32}$ ergs s^{-1}, i.e., more than one order of magnitude above most other ROX flares. The amplitude of the flares is seen to be distributed according to a power law, as is the case in the Sun and in flare stars.

As such, X-rays appear to be the best tool so far to detect PMS or very young objects near molecular clouds. More generally, a high X-ray activity may be characteristic of the very early stages of stellar evolution for all types of stars. The X-ray emission and time variability may indicate the presence of (relatively) large magnetic fields (with flares then arising from magnetic field reconnection) on these young and highly convective stars. This is perhaps connected with rotation, and in this case, the X-ray activity is expected to decay with age, unless the sources are close binaries (flare stars).

Also, this activity has presumably had a strong influence on the environment. The presence of numerous sources of X-rays, scattered within the cloud, affects strongly its ionization balance. On the other hand, it is highly probable that low-energy (MeV) particles are copiously injected in the circumstellar cavities created by the strong winds known to be emitted in general by PMS objects. Under certain conditions, still to be worked out, a weak intrinsic γ-ray emission may result.

Future work will be oriented more toward the various connections between the stars and the cloud. From this and previous works, it appears that soft X-rays are definitely a new major component of star formation regions. In the near future (until the AXAF mission takes over), planned EXOSAT observations as well as ongoing observations at other wavelengths will hopefully help to assess a number of points we have raised.

T. M., L. K.-M., and E. F. thank Fred Seward for his help in getting acquainted with the data processing system of the *Einstein Observatory*, and the data aides for having assisted them in handling up to 17 image files simultaneously, especially before Christmas 1981. We thank also Dan Fabricant, Rick Harnden, and Dan Harris for tireless advice. Useful discussions with Eric Feigelson, Mark Giampapa, Leon Golub, Bob Stern, and Giuseppe Vaiana are also gratefully acknowledged. We benefited from a useful correspondence with Jay Elias, and from his permission to use unpublished data, and also from comments by Giovanni Bignami on the manuscript. This reasearch was supported in part by the French Ministère des Relations Extérieures.

REFERENCES

Antiochos, S. K., and Sturrock, P. A. 1976, *Solar Phys.*, **49**, 359.
Bertout, C., and Thum, C. 1982, *Astr. Ap.*, **107**, 368.
Bignami, G. F., and Hermsen, W. 1983, *Ann. Rev. Astr. Ap.*, in press.
Boissé, P., *et al.* 1981, *Astr. Ap.*, **94**, 265.
Caraveo, P. A., *et al.* 1980, *Astr. Ap.*, **91**, L3.
Cassé, M., and Paul, J. A. 1980, *Ap. J.*, **237**, 236.
Chini, R., *et al.* 1977, *Astr. Ap.*, **56**, 323.
Cohen, M., Bieging, J. H., and Schwartz, P. R. 1982, *Ap. J.*, **253**, 707.
Cohen, M., and Kuhi, L. V. 1979, *Ap. J. Suppl.*, **41**, 743.
Cram, L. E. 1982, *Ap. J.*, **253**, 768.
De Campli, W. M. 1981, *Ap. J.*, **244**, 124.
Dolidze, M. V., and Arakelyan, M. A. 1959, *Sov. Astr.—AJ*, **3**, 434.
Drake, J. F. 1971, *Solar Phys.*, **16**, 152.
Elias, J. H. 1978, *Ap. J.*, **224**, 453.
Encrenaz, P., Falgarone, E., and Lucas, R. 1975, *Astr. Ap.*, **44**, 73.
Falgarone, E. 1979, Ph.D. thesis, Université de Paris VII.
Falgarone, E., and Gilmore, W. 1981, *Astr. Ap.*, **95**, 32.
Feigelson, E. D. 1982, *Icarus*, in press.
Feigelson, E. D., and De Campli, W. M. 1981, *Ap. J.* (*Letters*), **243**, L89.
Feigelson, E. D., and Kriss, G. A. 1981, *Ap. J.* (*Letters*), **248**, L35.
Felli, M., Gahm, G. F., Harten, R. H., Liseau, R., and Panagia, N. 1982, *Astr. Ap.*, **107**, 354.
Gabriel, A. H., *et al.* 1981, *Ap. J.* (*Letters*), **244**, L147.
Gahm, G. F. 1980, *Ap. J.* (*Letters*), **242**, L163.
Gahm, G. F., and Krautter, J. 1982, *Astr. Ap.*, in press.
Giacconi, R., *et al.* 1979, *Ap. J.*, **230**, 540.
Giacconi, R., *et al.* 1981, in *Telescopes for the 1980s*, ed. G. Burbidge and A. Hewitt (Palo Alto: Annual Reviews Inc.).
Giampapa, M. S., Calvet, N., Imhoff, C., and Kuhi, L. V. 1981, *Ap. J.*, **251**, 113.
Gorenstein, P. 1981, *Proc. 17th Int. Cosmic Ray Conf.* (Paris), **12**, 99.
Gorenstein, P., Harnden, F. R., Jr., and Fabricant, D. G. 1981, *I.E.E.E. Trans.*, **NS-28**, 869.
Grasdalen, G. L., Strom, K. M., and Strom, S. E. 1973, *Ap. J.* (*Letters*), **814**, L53.
Haisch, B. M., *et al.* 1977, *Ap. J.* (*Letters*), **213**, L119.
Haisch, B. M., *et al.* 1980, *Ap. J.* (*Letters*), **242**, L99.
Halpern, J. P., and Grindlay, J. E. 1980, *Ap. J.*, **242**, 1041.
Herbig, G. H., and Rao, N. K. 1972, *Ap. J.*, **174**, 401.
Kahler, S., *et al.* 1982, *Ap. J.*, **252**, 239.
Kahn, S. M., *et al.* 1979, *Ap. J.* (*Letters*), **234**, L107.
Krolik, J. H., and Kallman, T. R. 1983, *Ap. J.*, **267**, 610.
Ku, W. H. M., and Chanan, G. A. 1979, *Ap. J.* (*Letters*), **234**, L59.
Ku, W. H. M., Righini-Cohen, G., and Simon, M. 1982, *Science*, **215**, 61.
Kuan, P. 1976, *Ap. J.*, **210**, 129.

Kunkel, W. E. 1973, *Ap. J. Suppl.*, **25**, 1.
Kutner, M. L., Tucker, K. D., Chin, G., and Thaddeus, P. 1977, *Ap. J.*, **215**, 521.
Lada, C. J., and Wilking, B. A. 1980, *Ap. J.*, **238**, 620.
———. 1982, preprint.
Lamers, H. J. G. L. M. 1981, *Ap. J.*, **245**, 593.
McCray, R. 1982, private communication.
McWhirter, R. W. P., Thonemann, P. C., and Wilson, R. 1975, *Astr. Ap.*, **40**, 63.
Montmerle, T., and Cesarsky, C. 1981, *Proc. Int. School and Workshop on Plasma Astrophysics* (Varenna), ESA *SP-161*, 319.
Montmerle, T., Koch-Miramond, L., and Grindlay, J. E. 1981*a*, *Proc. 17th Int. Cosmic Ray Conf.* (Paris), **1**, 162.
———. 1981*b*, *Proc. 17th Int. Cosmic Ray Conf.* (Paris), **1**, 166.
Moore, R., *et al.* 1980, in *Solar Flares*, ed. P. Sturrock (Boulder: Colorado Associated University Press), p. 341.
Mullan, D. J. 1979, *Ap. J.*, **234**, 588.
Mundt, R., and Giampapa, M. S. 1982, *Ap. J.*, **256**, 156.
Myers, P. C., *et al.* 1978, *Ap. J.*, **220**, 864.
Nakazawa, K., and Nakagawa, Y. 1981, *Prog. Theoret. Phys. Suppl.*, **70**, 11.
Pallavicini, R., *et al.* 1981, *Ap. J.*, **248**, 279.
Panagia, N. 1973, *Astr. J.*, **78**, 929.
Paul, J. A., Cassé, M., and Montmerle, T. 1981, in *IAU Symposium 94, Origin of Cosmic Rays*, ed. G. Setti, G. Spada, A. W. Wolfendale (Dordrecht: Reidel), p. 325.
Pérault, M., and Falgarone, E. 1982, in *Regions of Recent Star Formation*, ed. R. S. Roger and P. E. Dewdney (Dordrecht: Reidel), p. 315.
Pollock, A. M. T., *et al.* 1981, *Astr. Ap.*, **94**, 116.
Pravdo, S. H., and Marshall, F. E. 1981, *Ap. J.*, **248**, 591.
Priest, E. R. 1981, in *Solar Flare Magnetohydrodynamics*, ed. E. R. Priest (New York: Gordon and Breach), p. 139.
Raymond, J. C. 1979, unpublished.
Raymond, J. C., Cox, D. P., and Smith, B. W. 1976, *Ap. J.*, **204**, 290.
Rosner, R., and Vaiana, G. S. 1978, *Ap. J.*, **222**, 1104.
Rydgren, A. E. 1980, *A.J.*, **85**, 438.
Scarsi, L., *et al.* 1977, in *Proc. 12th ESLAB Symposium, Recent Advances in γ-Ray Astronomy*, ESA **SP-124**, 3.
Stern, R. 1982, invited paper presented at XXIV *COSPAR* Meeting, Ottawa.
Struve, O., and Rudkjøbing, M. 1949, *Ap. J.*, **109**, 92.
Swanenburg, B., *et al.* 1981, *Ap. J.* (*Letters*), **243**, L49.
Vaiana, G. S. 1981, *Space Sci. Rev.*, **30**, 151.
Vaiana, G. S., *et al.* 1981, *Ap. J.*, **244**, 163.
Völk, H. J., and Forman, M. 1982, *Ap. J.*, **253**, 188.
Völk, H. J., Morfill, G. E., and Forman, M. 1981, *Ap. J.*, **249**, 161.
Vrba, F. J., Strom, K. M., Strom, S. E., and Grasdalen, G. L. 1975, *Ap. J.*, **197**, 77.
Vrba, F. J., Strom, S. E., and Strom, K. M. 1976, *A.J.*, **81**, 958.
Walter, F. M., and Kuhi, L. V. 1981, *Ap. J.*, **250**, 254.
Worden, S. P., Schneeberger, T. J., Kuhn, J. R., and Africano, J. L. 1981, *Ap. J.*, **244**, 520.

EDITH FALGARONE: DERIRM, Observatoire de Meudon, 92190 Meudon, France

JONATHAN GRINDLAY: Center for Astrophysics, 60 Garden Street, Cambridge, MA 02138

LYDIE KOCH-MIRAMOND and THIERRY MONTMERLE: DPh/EP/Ap, CEN SACLAY, 91191 Gif-sur-Ÿvette, Cedex, France

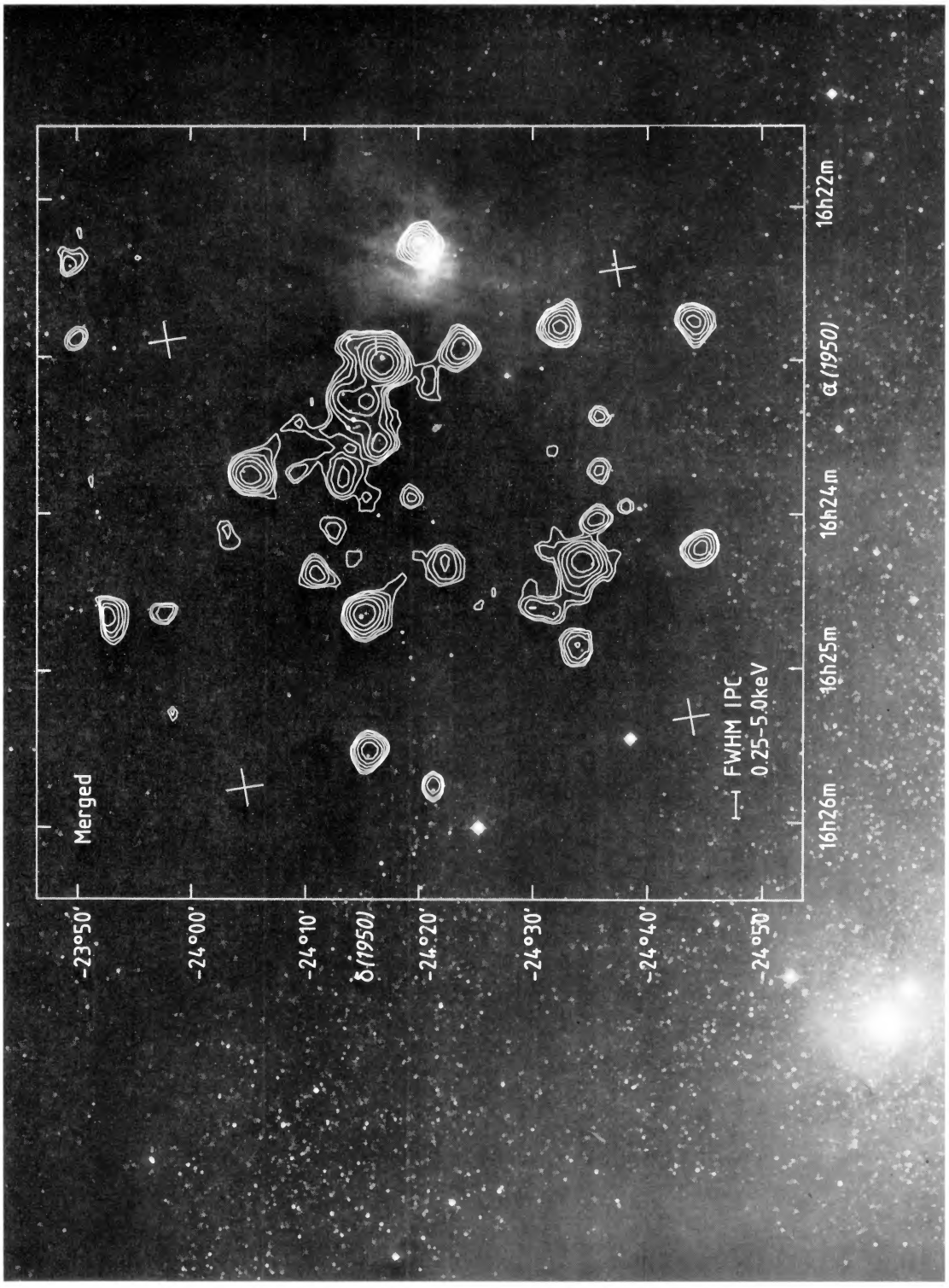

FIG. 2.—Same as Fig. 1, but with contours corresponding to the sum of exposures 1–6 (merged image), superimposed on a Palomar Sky Survey red print. (Note that the bright B2V star on the right, HD 147889, is *not* an X-ray source, after the revised processing; this is established by the HRI data. See also text, § VII*c*.)

PLATE 2

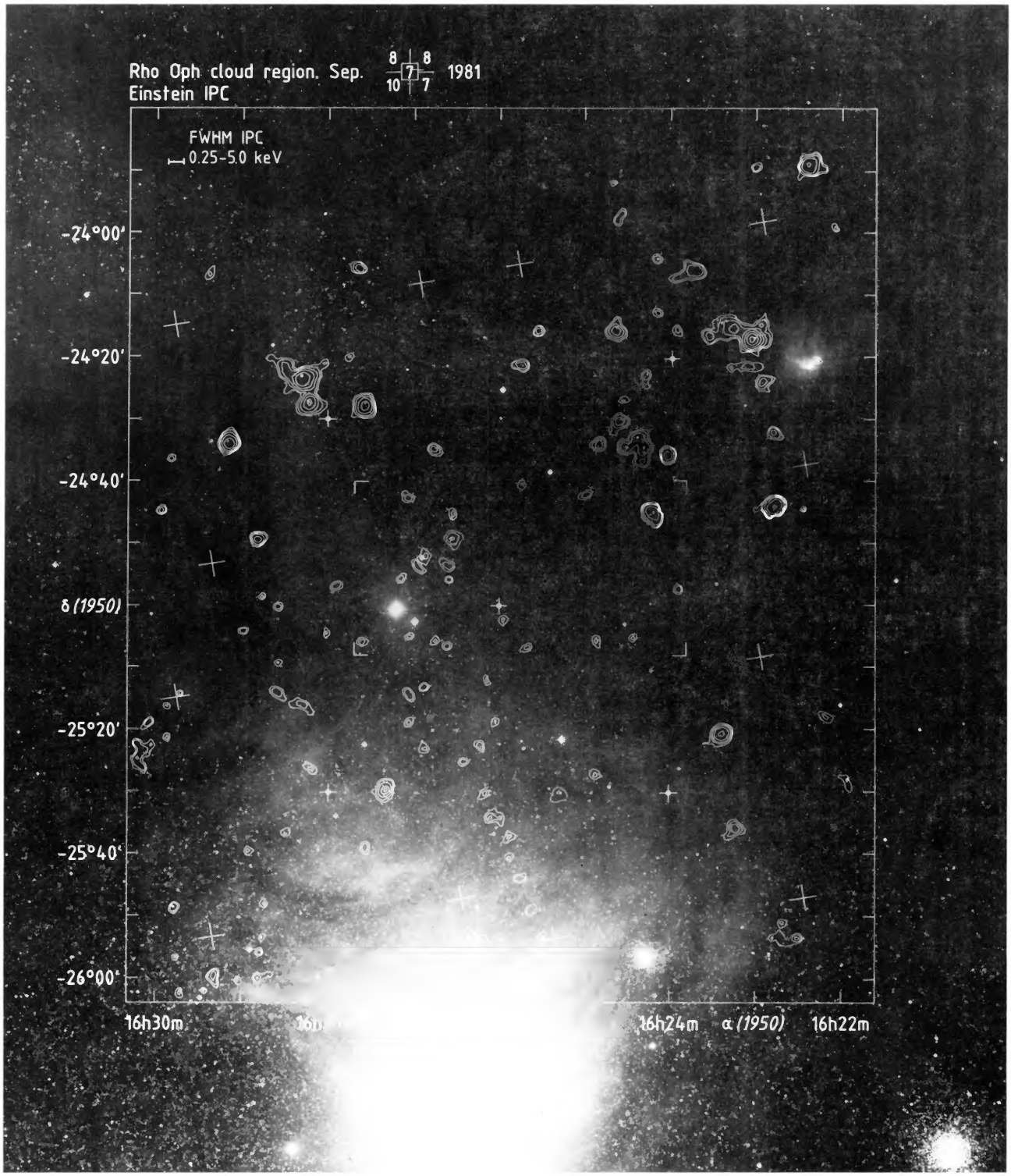

FIG. 3*a*

FIG. 3.—Overlays of the mosaic of five IPC fields covering the *COS B* error box for 2CG 353+16, on a PSS red print. The exact observation times for the IPC images differ typically by at least several hours: because of variability, these overlays are *not* snapshots of the entire field. Single contours were suppressed. Observation dates: Fig. 3*a*, 1979 September 7–10; Fig. 3*b*, 1981 February 7. The brightest source at that time is ROX-20; see text, §§ V and VI. Large crosses refer to the intersections of the IPC ribs; circled crosses refer to the observation axes. The part of the "middle" field shown is delimited by squares. The contours have the same meaning as in Fig. 1.

MONTMERLE *et al.* (*see* page 187)

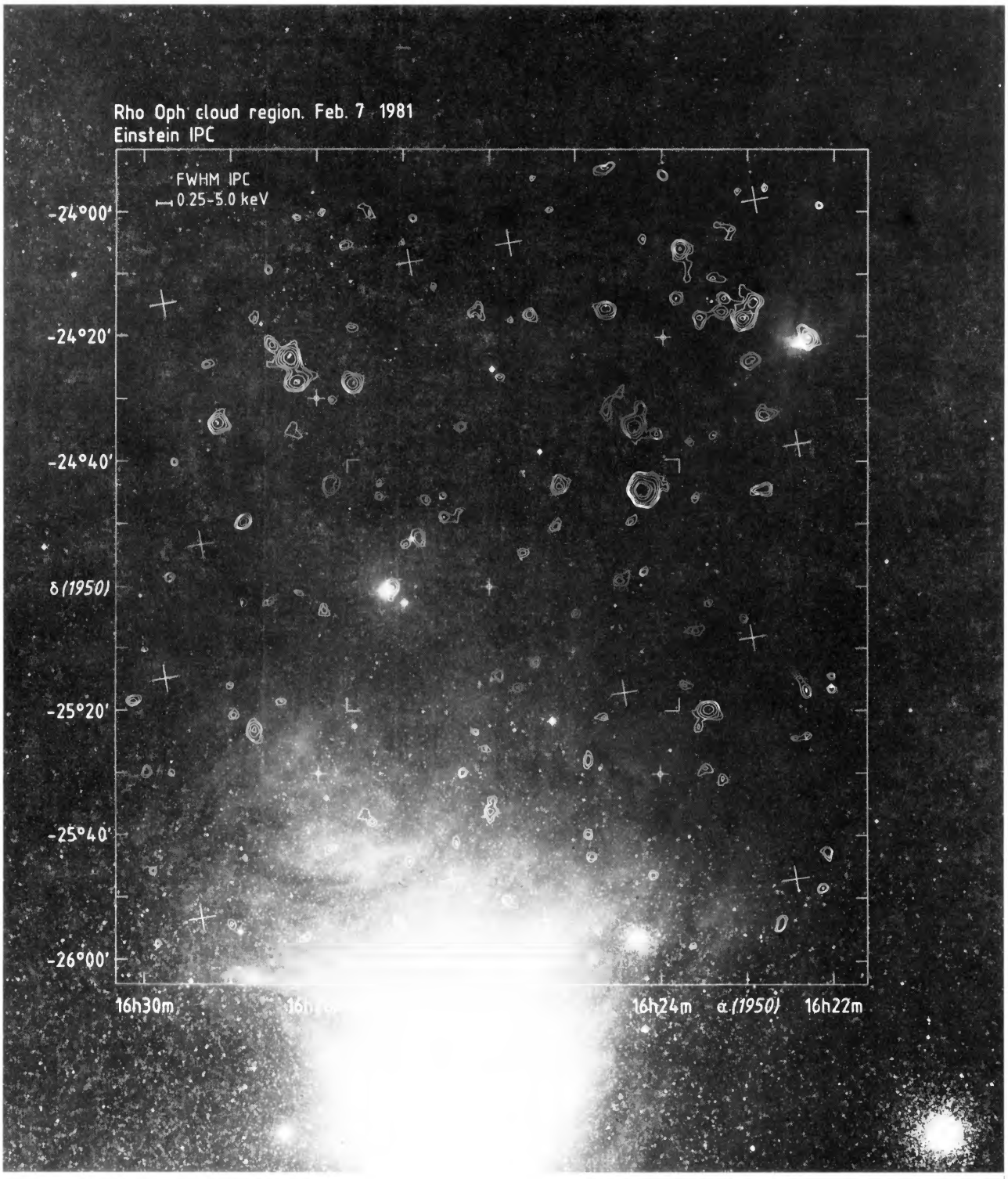

FIG. 3*b*

MONTMERLE *et al.* (*see* page 187)

PLATE 4

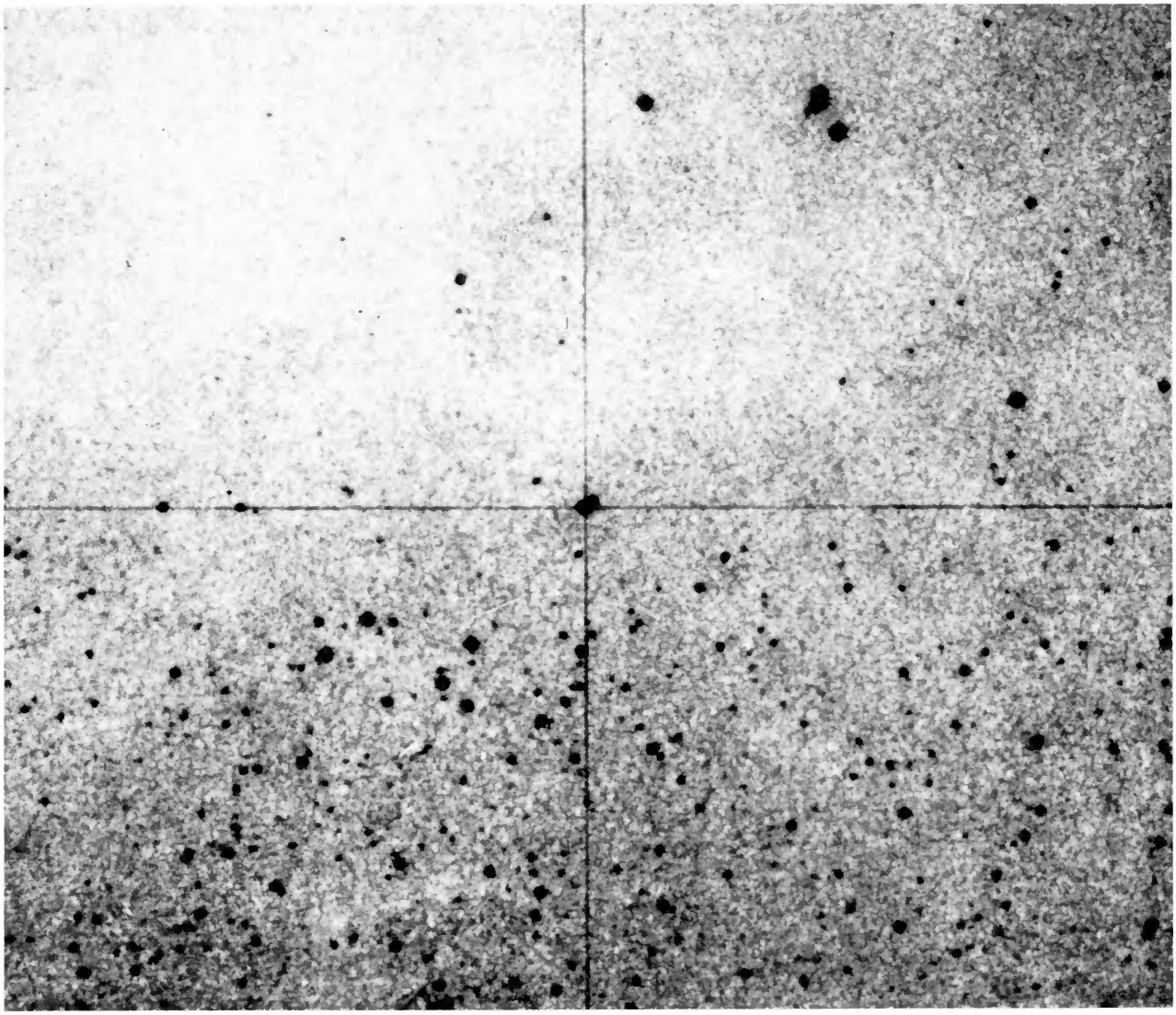

FIG. 7.—PSS red print of the region surrounding the source ROX-20 (*crosshairs*). This region is located at the southern edge of the dense part of the ρ Oph cloud. The star with a fuzzy appearance at the NNW of ROX-20 is the T Tau star SR24, also detected in the present investigation (see Table 2). North is at top. The two components, which the IPC cannot resolve, are ROX 20-1 (NW) and ROX 20-2 (SE); see Table 1.

MONTMERLE *et al.* (*see* page 192)